AD-A044 940 DAVID W TAYLOR NAVAL SHIP RESEARCH AND DEVELOPMENT CE--ETC F/G 20/4
A DISCRETE VORTEX METHOD FOR PREDICTING HYDRODYNAMIC LOADS ON S--ETC(U)
SEP 77 T C TAI, R E WHITEHEAD

UNCLASSIFIED AERO-1240 DTNSRDC-77-0035 NL

1 OF 1
ADA044940

END
DATE FILMED
11-77
DDC

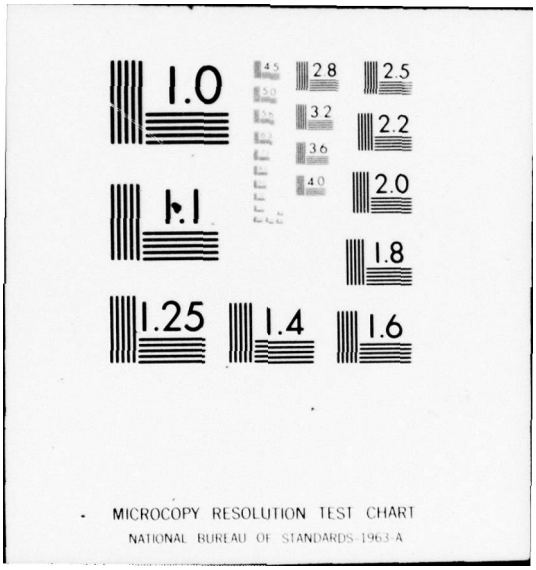
1.0
1.1
1.25
1.4
1.6
1.8
2.0
2.2
2.5
2.8
3.2
3.6
4.0
4.5
5.0
MICROCOPY RESOLUTION TEST CHART
NATIONAL BUREAU OF STANDARDS-1963-A

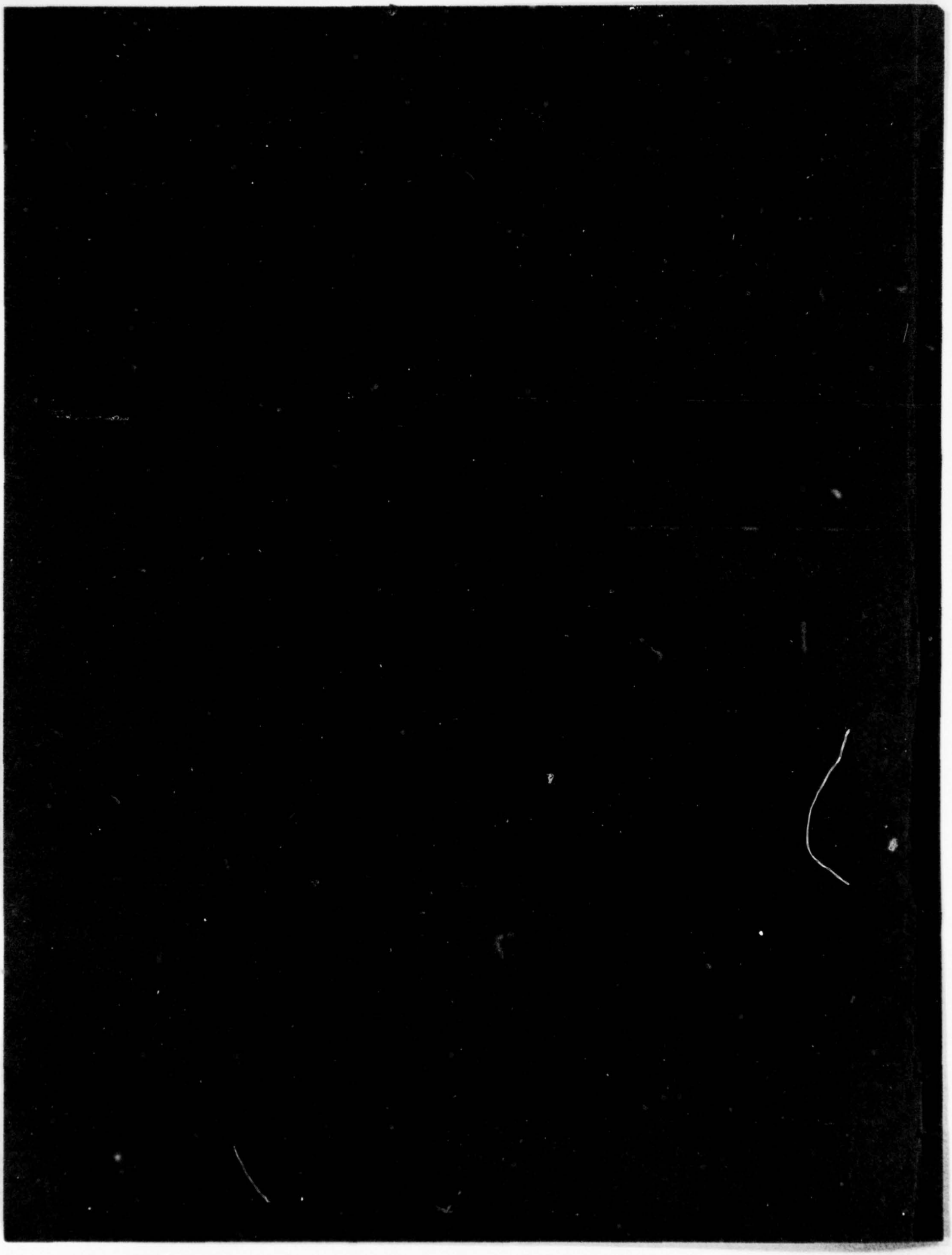

UNCLASSIFIED

SECURITY CLASSIFICATION OF THIS PAGE (When Data Entered)

REPORT DOCUMENTATION PAGE

READ INSTRUCTIONS BEFORE COMPLETING FORM

1. REPORT NUMBER: DTNSRDC-77-0035
2. GOVT ACCESSION NO.
3. RECIPIENT'S CATALOG NUMBER

4. TITLE (and Subtitle): A DISCRETE VORTEX METHOD FOR PREDICTING HYDRODYNAMIC LOADS ON SIDEWALLS OF SURFACE EFFECT SHIPS.

5. TYPE OF REPORT & PERIOD COVERED: Interim Report. Jul 1975-Dec 1976.

6. PERFORMING ORG. REPORT NUMBER: Aero Report-1240

7. AUTHOR(s): Tsze C. Tai and Robert E. Whitehead

8. CONTRACT OR GRANT NUMBER(s): SR0230101

9. PERFORMING ORGANIZATION NAME AND ADDRESS
David W. Taylor Naval Ship Research and Development Center
Bethesda, Maryland 20084

10. PROGRAM ELEMENT, PROJECT, TASK AREA & WORK UNIT NUMBERS
Program Element 61153N
Task SR0230101
Work Unit 1-1606-040

11. CONTROLLING OFFICE NAME AND ADDRESS
Naval Sea Systems Command
Code SEA 035
Washington, D.C. 20362

12. REPORT DATE: September 1977

13. NUMBER OF PAGES: 64 (62p.)

14. MONITORING AGENCY NAME & ADDRESS (if different from Controlling Office)
Ship Performance Department
David W. Taylor Naval Ship R&D Center
Bethesda, Maryland 20084

15. SECURITY CLASS. (of this report): UNCLASSIFIED

15a. DECLASSIFICATION/DOWNGRADING SCHEDULE

16. DISTRIBUTION STATEMENT (of this Report)

APPROVED FOR PUBLIC RELEASE: DISTRIBUTION UNLIMITED

17. DISTRIBUTION STATEMENT (of the abstract entered in Block 20, if different from Report)

DDC RECEIVED OCT 4 1977 C

18. SUPPLEMENTARY NOTES

19. KEY WORDS (Continue on reverse side if necessary and identify by block number)
Surface Effect Ships
Hydrodynamic Loads
Discrete Vortex Method
Sidewalls

20. ABSTRACT (Continue on reverse side if necessary and identify by block number)

A discrete vortex method ~~has been~~ was formulated for calculating the hydrodynamic loads on SES sidewalls in an inviscid separated flow due to vorticity. A rigid, flat, free surface is assumed. The vortex system consists of a bound vortex lattice attached on the lifting surface, a single free tip vortex core from the side edge, and free vortex lines emanating from the trailing edge. The presence of these free vortices accounts for -> next page

(Continued on reverse side)

DD FORM 1 JAN 73 1473 EDITION OF 1 NOV 65 IS OBSOLETE
S/N 0102-LF-014-6601

UNCLASSIFIED
SECURITY CLASSIFICATION OF THIS PAGE (When Data Entered)

LB

387 695

(Block 20 continued)

cont. the nonlinear effects. Single and double sidewalls of different area aspect ratios ~~have been~~ were considered for various geometrical arrangements and flow conditions. It was found that with the present single tip vortex model, the accuracy of the results improved with increasing aspect ratio. Side forces predicted for small AR cases were higher than given by other methods. The effect of wall interference was significant for double sidewalls with increases in length-to-beam ratio, or area aspect ratio, or yaw angle.

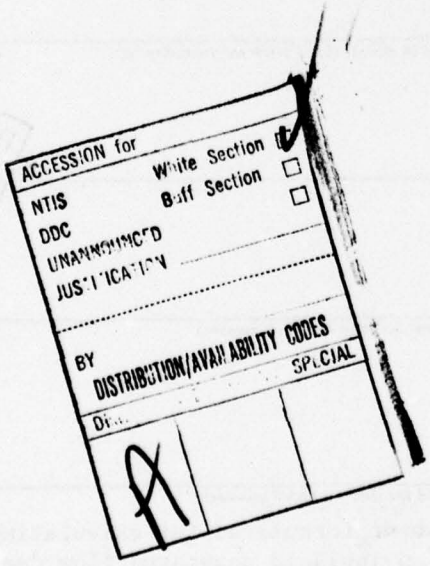

TABLE OF CONTENTS

LIST OF FIGURES

NOTATION

AR	Area aspect ratio
C_D	Drag coefficient
C_L	Side force coefficient
C_m	Yaw moment coefficient
C_N	Normal force coefficient
C_P	Pressure coefficient
C.P.	Center of pressure
c	Length of sidewall
$\bar{c}_1, \bar{c}_2$	Diagonal vector as defined in Equations (25) and (26)
B	Distance between two sidewalls
b	Width of sidewall
$\bar{e}$	Unit vector
$\bar{F}$	Force
f_x, f_y, f_z	Force components in x, y, z direction
G,g	Geometrical functions
h	Distance between the segment of a sender and the control point of a receiver
$\bar{i}, \bar{j}, \bar{k}$	Vectors along x, y, z coordinates
L	Length of vortex segment
N	Number of vortex segments
$\bar{n}$	Normal vector
R	Normal component of free-stream velocity
$\bar{r}_p, \bar{r}_q, \bar{r}_s$	Position vectors of the control point of a receiver with respect to the ends of the segment of a sender
$\bar{V}$	Velocity

x,y,z	Cartesian coordinates
α	Yaw angle
β	Pitch angle
γ	Circulation
θ	Angles used in the Biot-Savart law
ρ	Fluid density

Subscripts

b	Bound vortex
c/4	Quarter chord of a side wall
e	Tip vortex
i	Image, initial location of tip vortex core
K,k,M,N	Indices
ℓ	Longitudinal
n	Normal
O	Control point
qp,qs	Parallel to the spanwise and chordwise vortex segment
t	Transverse
v	Parallel to the velocity
w	Wake vortex
∞	Free-stream condition

ABSTRACT

A discrete vortex method has been formulated for calculating the hydrodynamic loads on SES sidewalls in an inviscid separated flow due to vorticity. A rigid, flat, free surface is assumed. The vortex system consists of a bound vortex lattice attached on the lifting surface, a single free tip vortex core from the side edge, and free vortex lines emanating from the trailing edge. The presence of these free vortices accounts for the nonlinear effects. Single and double sidewalls of different area aspect ratios have been considered for various geometrical arrangements and flow conditions. It was found that with the present single tip vortex model, the accuracy of the results improved with increasing aspect ratio. Side forces predicted for small AR cases were higher than given by other methods. The effect of wall interference was significant for double sidewalls with increases in length-to-beam ratio, or area ratio, or yaw angle.

ADMINISTRATIVE INFORMATION

This work was authorized by the Naval Sea Systems Command (SEA 035) and funded through the General Hydromechanics Research Program under Task SR0230101, Work Unit 1-1606-040. The study was conducted by Codes 1606 and 1615 and monitored by Code 1506, David W. Taylor Naval Ship Research and Development Center (DTNSRDC).

INTRODUCTION

Recent improvements in surface effect ships (SES) have been aimed at higher performance operations of SES's with high length-to-beam ratios. The sidewalls of such crafts are subject to severe side forces and moments which sometimes become detrimental to maneuverability. Acting as low-aspect-ratio lifting bodies, the hydrodynamic loads on those sidewalls are greatly influenced by the presence of vortices created by flow separation from the leading and side edges of the surface.

The problem is essentially nonlinear because of the free vortex influence. Even though flow separation exists, the flow field can still be analyzed by using an inviscid model when separation occurs only along the sharp edges. Limited theoretical work has already been performed

in this area. Whitehead[1] developed a simplified model by assuming a rigid free surface on the upper ends of the sidewalls and neglecting the effects of cushion pressure and seals. Lamar[2] used a generalized suction analogy to predict force contributions due to the vortices shed from the sidewalls. In conjunction with the side-edge suction analogy, Woodward et al.[3] obtained the required pressure distribution from a separate three-dimensional, lifting surface theory of attached potential flow. They found reasonable results for rectangular parallel sidewalls with aspect ratios of 0.1 and 0.2, but did not determine the location of the shedding vortices because of the limitation of the side-edge suction analogy. This same limitation precluded calculating the influence of one sidewall when a vortex is shed from an adjacent sidewall. The use of linear potential flow theory also raises some questions for cases with aspect ratios of 0.1 or less.

Wilson[4] also employed the generalized suction analogy but he calculated the required pressure distributions from slender wing theory rather than linear potential flow theory. For most cases, his results on net side force and moment compared fairly well with those obtained by Whitehead.[1] However the two approaches gave different trends for force and moment coefficients on each individual wall as affected by interference due to spacing.

The present work considers the problem of two parallel sidewalls at a constant yaw angle and utilizes a discrete vortex method to simulate

---

[1]Whitehead, R.E., "A Theoretical Prediction Technique for Lateral Hydrodynamic Loads on Sidewalls of Surface Effect Ships," DTNSRDC Report 4766 (Dec 1975). A complete list of references is given on page 55.

[2]Lamar, J.E., "Extension of Leading-Edge Suction Analogy to Wings with Separated Flow Around the Side Edges at Subsonic Speeds," NASA TR 428 (Oct 1974).

[3]Woodward, R.A. et al., "A Computer Program for Three-Dimensional Lifting Bodies in Subsonic Inviscid Flow," United States Army Air Mobility R&D Laboratory Report TR-74-18 (Apr 1974).

[4]Wilson, M.B., "Interference Effects on Lateral Forces and Moments on High L/B SES Arrangements," Paper 76-859 presented at the AIAA/SNAME Advanced Marine Vehicles Conference, Arlington, Virginia (Sep 1976).

the lifting surface of the sidewalls and the shedding of vortices from the side edge of the sidewall surface. The nonlinear effect of flow separation from sharp edges is accounted for by considering the free tip and wake vortex cores away from the surface. For simplicity the tip vortices are represented by a single free-vortex core which is merged by side edge vortices a short distance away from the wall. An iterative procedure is employed to obtain the direction of the core as well as the wake vortices in the solution.

VORTEX FLOW MODELS

SINGLE-WALL MODEL

First, we consider the problem of an SES with a flat wall of finite aspect ratio traveling in calm water. The upper end of the wall is aligned with the surface of the water. With the assumption of a rigid free surface, the flow can be simulated by a bound vortex sheet and free vortex sheets emanating from the side and trailing edges of the wall. A schematic of the flow is shown in Figure 1. The yaw angle α is measured with respect to the x-z plane. The $z = 0$ plane is assumed to be flat and rigid, and its influence is represented by an image in the (-z) region.

The vortex system of the subject boundary value problem consists of a bound vortex sheet attached on the lifting surface, a free edge vortex sheet rolling up from the side edge, and a free wake vortex sheet emanating from the trailing edge; see Figure 1. There is a pressure difference across a bound vortex sheet but not across a free vortex sheet. However, the normal component of velocity vanishes on either a bound or free vortex sheet.

The present single-wall arrangement is similar to that of Kandil[5] except that the tip vortex sheets have been simplified to a single vortex core and that no vortex segment is placed along the side edge in order to satisfy the Kutta condition there.

---

[5]Kandil, O.A., "Prediction of the Steady Aerodynamic Loads on Lifting Surfaces Having Sharp-Edge Separation," Ph.D. Thesis, Virginia Polytechnic Institute and State University, Blacksburg, Virginia (Dec 1974).

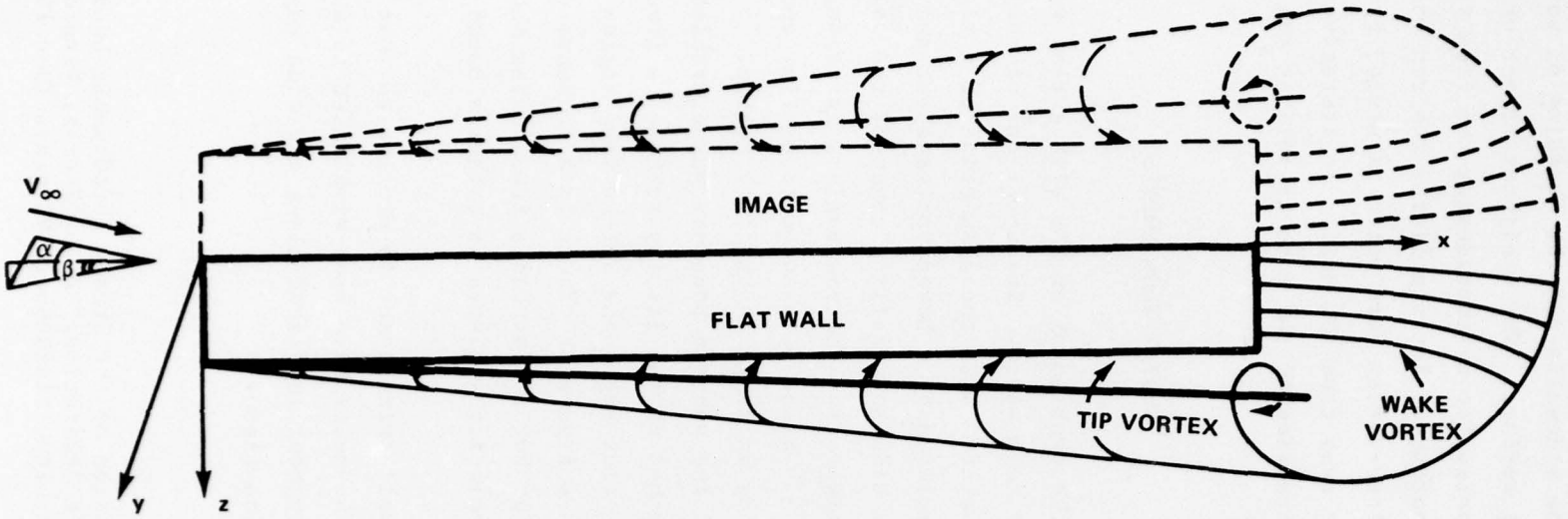

Figure 1 - Flow Past a Single Flat Wall with Upper End Aligned with a Flat Free Surface

DOUBLE-SIDEWALL MODEL

In practical SES's, there are always two sidewalls placed side by side and separated by a finite distance. To simplify the problem, it is assumed that the effect of the cushion pressure and seals can be neglected. The problem is then reduced to two distinct single walls with mutual interference. The schematic of the vortex system for the two-sidewall model is shown in Figure 2. As for the single-wall case, it is assumed that the free surface is rigid and flat and that its influence is accounted for by the vortex images in the (-z) region.

Mutual interference results from the presence of a vortex field in both sidewalls. The velocity at a control point has to be calculated by considering the contributions of the vortex elements not only from a single sidewall but also from those of the adjacent sidewall a finite distance away. As a general rule, however, only those vortex elements that the control point can "see" make contributions. Because of the presence of the other wall, the shape of the vortex sheets of the upstream sidewall is also confined to limited space between the solid boundaries; however, this assumption is important only in the case of very narrow spacing and high yaw angles.

BASIC EQUATIONS

INDUCED VELOCITY

For an inviscid and incompressible fluid flow, the velocity generated by a vortex segment is determined by using the Biot-Savart law; see Figure 3. For a control point o_c in the presence of vortex segment qs with circulation γ, the induced velocity is given by

$$\bar{V} = \frac{\gamma}{4\pi h} \left(\cos \theta_1 + \cos \theta_2\right) \bar{e}_v \tag{1}$$

where

$$\cos \theta_1 = \frac{\bar{r}_q \cdot \bar{e}_{qs}}{|\bar{r}_q|} \tag{2}$$

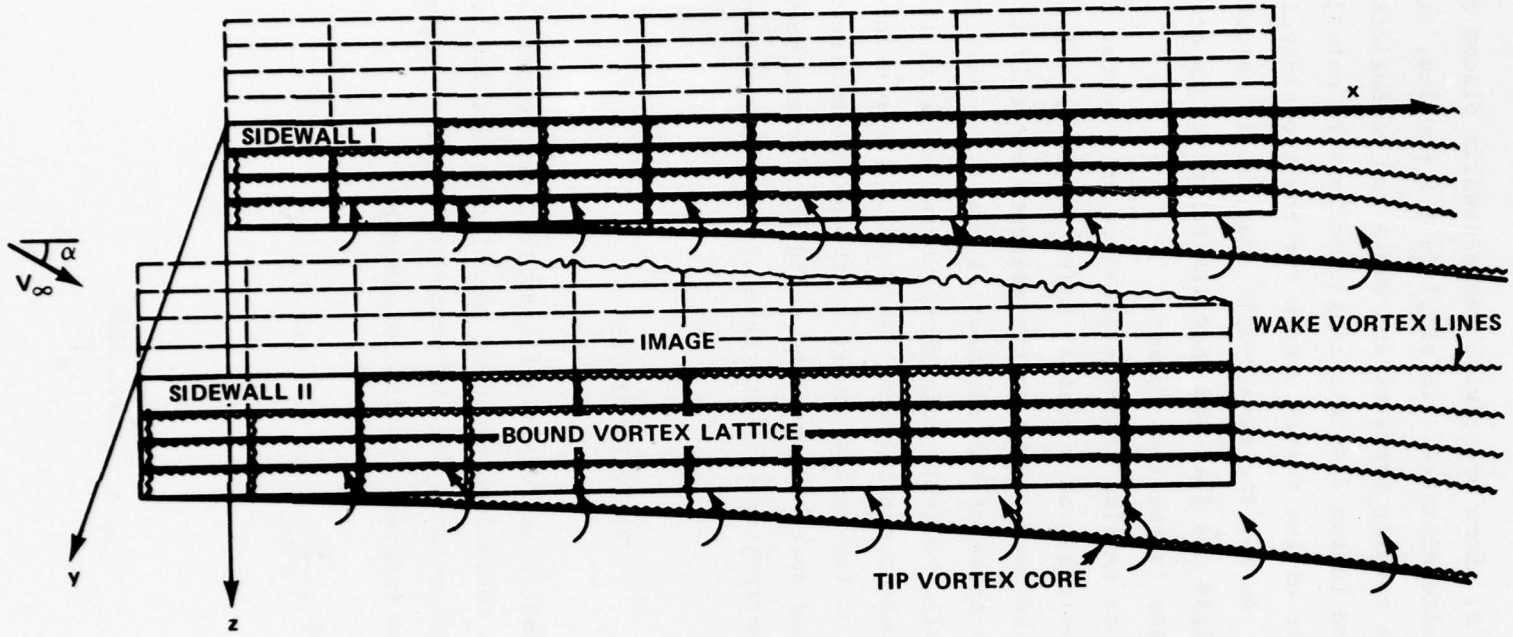

Figure 2 - The Vortex System for SES Sidewalls

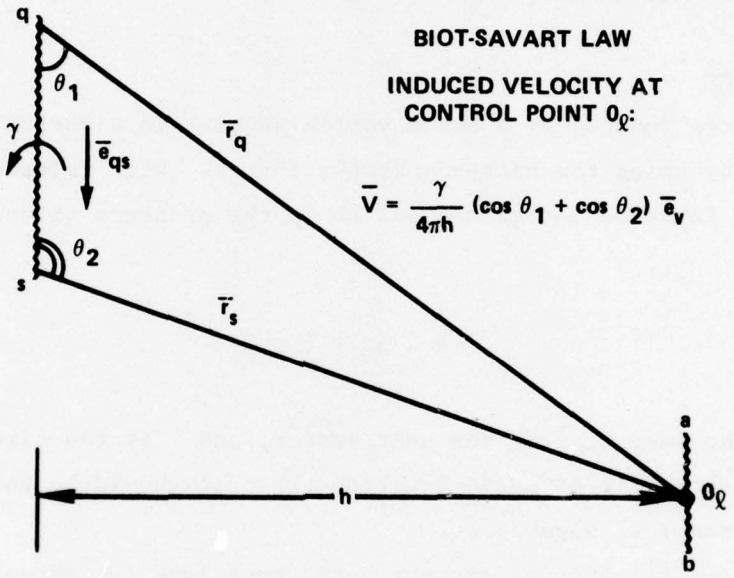

Figure 3 - Induced Velocity at a Vortex Segment According to Biot-Savart Law

and

$$\cos \theta_2 = - \frac{\bar{r}_s \cdot \bar{e}_{qs}}{|\bar{r}_s|} \tag{3}$$

Here $\bar{e}_v$ is the unit vector of the induced velocity and $\bar{e}_{qs}$ is the unit vector parallel to the vortex segment qs.

The derivation of Equation (1) can be found in standard text. As shown in Figure 4, a control point is used to apply the boundary condition only when necessary to determine the influence coefficients, as discussed later in the section on numerical procedure.

INDUCED FORCE

The force induced by a bound vortex segment in a vortex field can be calculated by using the Kutta-Joukowski theory. With reference to Figure 5, the induced force on vortex segment ab in the presence of vortex segment qs is given by

$$\bar{F} = \rho L \Gamma \bar{V} \times \bar{e} \tag{4}$$

Here L is the length, $\bar{e}$ is the unit vector, and Γ is the circulation of segment ab. $\bar{V}$ is given in Equation (1). It should be noted that Γ differs from γ of segment qs.

Equations (1) and (4) are the basic equations for computing the necessary flow characteristics of an inviscid and incompressible flow. They originate from the nonlinear partial differential equations governing a rotational flow, with the aid of the theorem of Stokes.[6] Flow separation caused by vortex rather than viscosity may take place. Such a situation may exist in a flow with angle of yaw up to 26 degrees, as observed experimentally.

At the surface of bound vortex sheets, the normal component of velocity vanishes and there is a pressure difference across the sheet; the boundary conditions are:

---

[6]Prandtl, L. and O.E. Tietjens, "Fundamentals of Hydro- and Aerodynamics," translated by L. Rosenhead, Dover Publications, New York (1957).

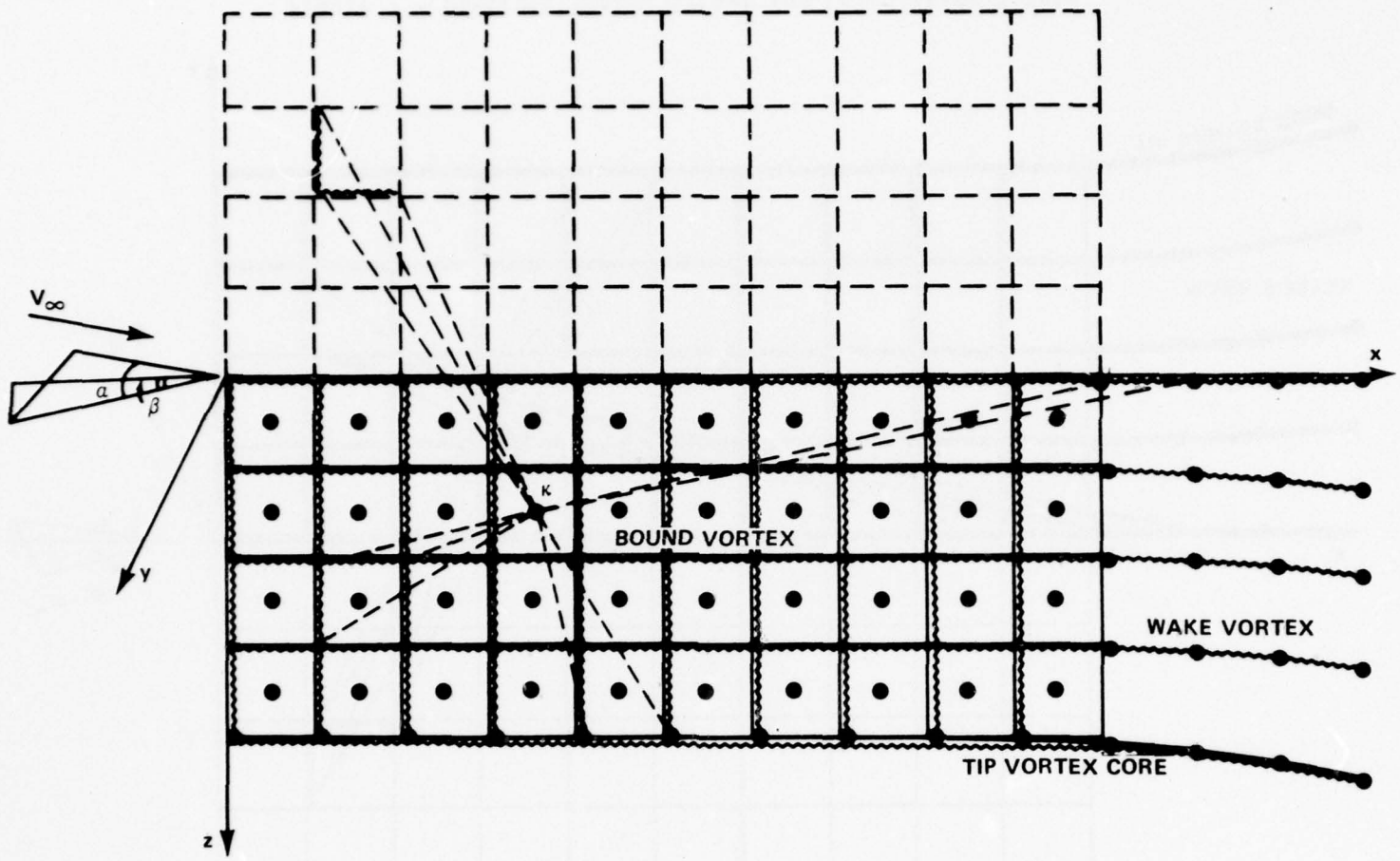

Figure 4 - Discrete Vortex System for Determining Circulation

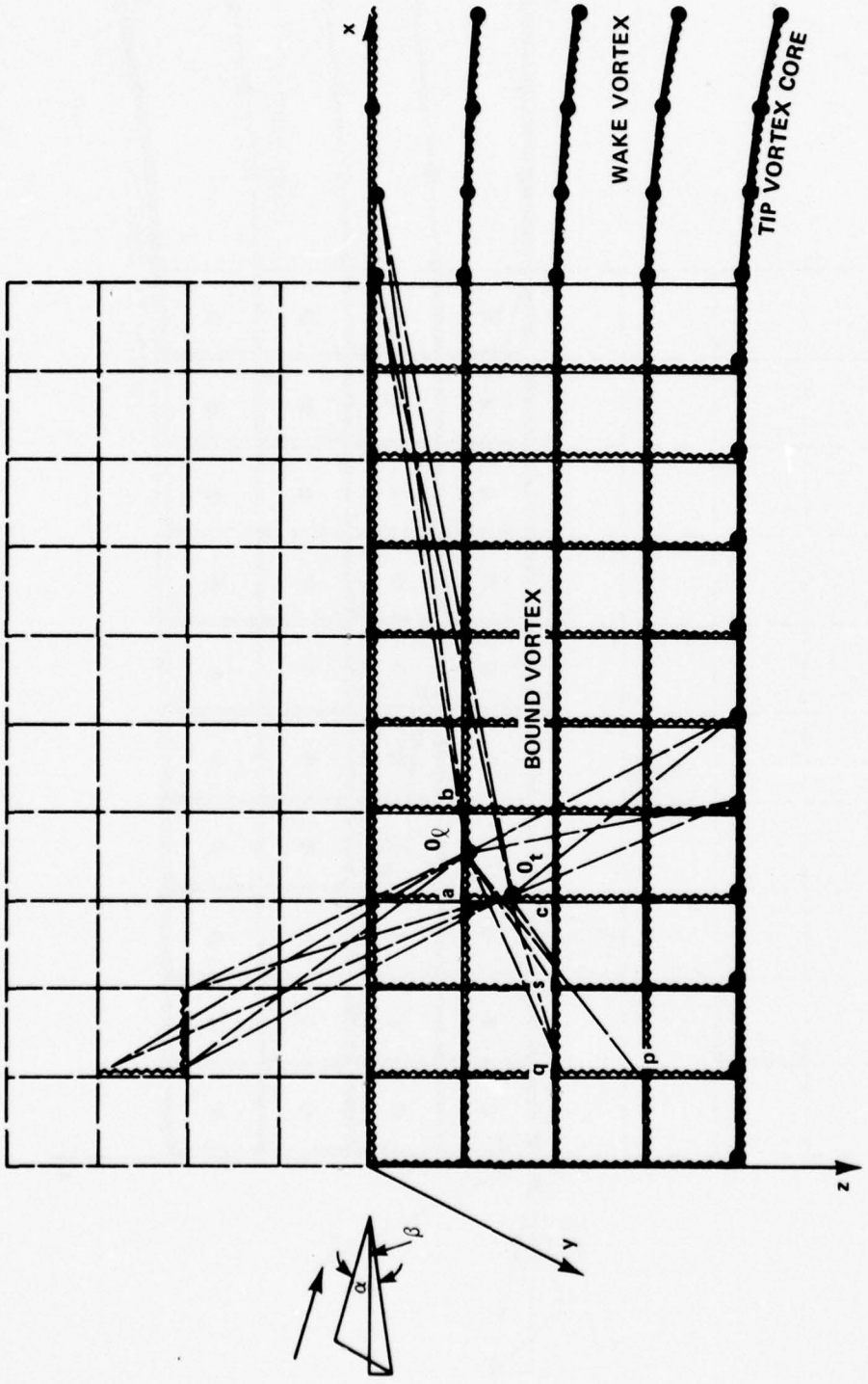

Figure 5 - Discrete Vortex System for Calculating Forces

$$\bar{n} \cdot \bar{V} = 0$$

$$\Delta C_p \neq 0 \tag{5}$$

At the trailing and side edges, however,

$$\Delta C_p = 0 \tag{6}$$

in order to satisfy the Kutta condition. The normal component of velocity also vanishes at the surface of a free vortex sheet but there is no pressure difference across a sheet and so the boundary conditions are:

$$\bar{n} \cdot \bar{V} = 0$$

$$C_p = 0 \tag{7}$$

DISCRETE VORTEX METHOD

The circulation values in Equations (1) and (4) are generally unknown and must be determined numerically in order to calculate the velocity and forces. For illustrative purposes, we consider the single-wall model first.

In the numerical procedure, a bound vortex sheet is represented by a lattice and a free vortex sheet by a series of nonintersecting lines. For simplicity, those nonintersecting free edge vortex lines that emanate at the end of each row of the vortex lattice are merged into a single vortex core at each side of the wall; see Figure 4. Both the free wake vortex lines and the free tip vortex cores are composed of a series of short vortex segments, except for the last segment which is semi-infinite and extends downstream parallel to the free stream. These segments are generally separated from the surface and their final location is determined by the solution with the aid of an iteration procedure. The force-free condition on the free vortex sheet is approximately satisfied by aligning

these segments with local streamlines. The presence of these free vortex segments accounts for the nonlinear relationship between yaw angle and force coefficients.

The lattice of the bound vortex divides the lifting surface into panels. Each panel has a spanwise vortex segment along its forward edge and a chordwise vortex segment along its inboard edge. The center of the panel is the control point at which the boundary condition of the vanishing normal velocity component $\bar{n} \cdot \bar{V} = 0$ applies. No vortex segment is placed along the trailing and side edges in order to satisfy the Kutta condition.

DETERMINATION OF CIRCULATION FIELD

When a cartesian coordinate system is used, then (see Figure 4) the velocity at the control point O_c will be the vector sum of contributions from all vortex segments in the field.

$$\bar{V}_{O_c} = \sum_{K=1}^{N_b} \left[\left(g_{t_K} \gamma_{t_K} + g_{ti_K} \gamma_{ti_K} \right) \bar{e}_{vt_K} + \left(g_{\ell_K} \gamma_{\ell_K} + g_{\ell i_K} \gamma_{\ell i_K} \right) \bar{e}_{v\ell_K} \right] \tag{8}$$

$$+ \sum_{M=1}^{N_t} \left(g_{e_M} \gamma_{e_M} + g_{ei_M} \gamma_{ei_M} \right) \bar{e}_{v\ell_M} + \sum_{N=1}^{N_w} \left(g_{w_N} \gamma_{w_N} + g_{wi_N} \gamma_{wi_N} \right) \bar{e}_{v\ell_N}$$

where N_b, N_t, and N_w are the number of vortex segments in the bound, tip, and wake vortex sheets, respectively. Subscript t denotes spanwise segments and ℓ, chordwise segments. Terms with subscript i are contributions from the image. Other variables are:

$$g_{t_K} = \frac{1}{4\pi h_{t_K}} \left(\cos \theta_{t1_K} + \cos \theta_{t2_K} \right) \tag{9}$$

$$g_{ti_K} = \frac{1}{4\pi h_{ti_K}} (\cos \theta_{til_K} + \cos \theta_{ti2_K}) \tag{10}$$

$$g_{\ell_K} = \frac{1}{4\pi h_{\ell_K}} (\cos \theta_{\ell 1_K} + \cos \theta_{\ell 2_K}) \tag{11}$$

$$g_{\ell i_K} = \frac{1}{4\pi h_{\ell i_K}} (\cos \theta_{\ell il_K} + \cos \theta_{\ell i2_K}) \tag{12}$$

$$g_{e_M} = \frac{1}{4\pi h_{e_M}} (\cos \theta_{el_M} + \cos \theta_{e2_M}) \tag{13}$$

$$g_{ei_M} = \frac{1}{4\pi h_{ei_M}} (\cos \theta_{eil_M} + \cos \theta_{ei2_M}) \tag{14}$$

$$g_{w_N} = \frac{1}{4\pi h_{w_N}} (\cos \theta_{wl_N} + \cos \theta_{w2_N}) \tag{15}$$

$$g_{wi_N} = \frac{1}{4\pi h_{wi_N}} (\cos \theta_{wil_N} + \cos \theta_{wi2_N}) \tag{16}$$

The variables θ and h are strictly geometrical properties which can be evaluated for a given configuration and vortex system arrangement. The detailed evaluation for these quantities is given in the appendix.

However, the values of circulation γ are still unknown at this stage. They will be determined as follows.

With the aid of the image principle, we write

$$\gamma_{ti_K} = \gamma_{t_K} \tag{17}$$

$$\gamma_{\ell i_K} = - \gamma_{\ell_K} \tag{18}$$

$$\gamma_{ei_M} = \gamma_{e_M} \tag{19}$$

$$\gamma_{wi_N} = - \gamma_{w_N} \tag{20}$$

From conservation of vortex at any spatial point, we have

$$\gamma_{\ell_K} = \gamma_{\ell_{K-N_z}} + \gamma_{t_{K+1}} - \gamma_{t_K} \tag{21}$$

as illustrated by the following sketch

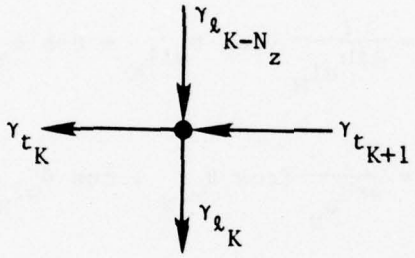

At the edge of the sidewall, the circulation of the tip vortex line at a given row equals that of the vortex segment adjoining the tip vortex core, i.e.,

$$\gamma_{e_M} = \gamma_{t_K} \text{ when } K = M\ N_z \tag{22}$$

as illustrated in the following sketch

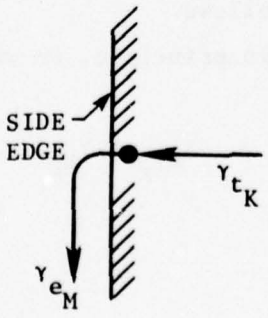

At the trailing edge, the circulation of the wake vortex line at a given column equals that of the vortex segment adjoining the wake vortex line and thus

$$\gamma_{w_N} = \gamma_{\ell_K} \text{ when } K > N_z\ (N_x - 1) \tag{23}$$

as illustrated by the following sketch

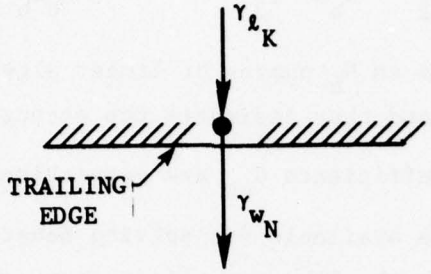

The unit normal vector at control point O_c (indexed by k for receiver) is

$$\bar{e}_n = \bar{c}_1 \times \bar{c}_2 / |\bar{c}_1 \times \bar{c}_2| \tag{24}$$

where

$$\bar{c}_1 = (x_3 - x_1)\bar{i} + (y_3 - y_1)\bar{j} + (z_3 - z_1)\bar{k} \tag{25}$$

$$\bar{c}_2 = (x_4 - x_2)\bar{i} + (y_4 - y_2)\bar{j} + (z_4 - z_2)\bar{k} \tag{26}$$

Here $\bar{i}$, $\bar{j}$, $\bar{k}$ are the base vectors in a cartesian coordinate system.

The normal component of velocity at point O_c is thus obtained by substituting Equations (8) and (24) into (5). After simplifying, we get

$$G_{k1}\,\gamma_{t_1} + G_{k2}\,\gamma_{t_2} + G_{k3}\,\gamma_{t_3} + \ldots G_{kN_b}\,\gamma_{t_{N_6}} + R_k = 0 \tag{27}$$

where G_k is a geometrical quantity and R_k is the normal component of the free stream velocity. Similarly, this equation holds for other points in the bound vortex lattice from k = 1 to N_b:

$$
\begin{aligned}
&G_{11}\,\gamma_{t_1} + G_{12}\,\gamma_{t_2} + G_{13}\,\gamma_{t_3} + \cdots + G_{1N_b}\,\gamma_{t_{N_b}} + R_1 = 0 \\
&G_{21}\,\gamma_{t_1} + G_{22}\,\gamma_{t_2} + G_{23}\,\gamma_{t_3} + \cdots + G_{2N_b}\,\gamma_{t_{N_b}} + R_2 = 0 \\
&\quad\vdots \\
&G_{N_b1}\,\gamma_{t_1} + G_{N_b2}\,\gamma_{t_2} + G_{N_b3}\,\gamma_{t_3} + \cdots + G_{N_bN_b}\,\gamma_{t_{N_b}} + R_{N_b} = 0
\end{aligned}
\tag{28}
$$

This equation gives an N_b number of linear algebraic equations for N_b number of unknowns γ_{t_K} and thus indicates the strength of the circulation. Again, the influence coefficients G_{kK} are geometrical properties. Several numerical procedures are available for solving Equation (28). The particular one employed here is the Gaussian elimination scheme without pivoting. (A Gauss-Seidel iteration scheme was also used for some checkout cases.) The solution gives the circulation values for γ_{t_K}. The values for γ_{ℓ_K}, γ_{e_M}, and γ_{w_N} can then be found with the aid of Equations (21) and (23).

DETERMINATION OF FREE VORTEX LINES

The geometrical properties represented by the influence coefficients depend strictly on the position of the vortex segments. For free vortex lines representing the free edge and wake vortex sheets, their positions coincide with the local streamlines which are determined by the solution. This is done through an iteration procedure.

The positions of free vortex lines are initially specified at the end of each row of the bound vortex lattice for the free tip vortex lines and at the end of each column for the free wake vortex lines. Since these lines are free of force, they will eventually align with the local streamlines, as mentioned previously. During the course of solution, therefore, the positions of those free vortex segments were updated by modifying their coordinates with increments in the direction of local velocity. The modified coordinates were then used to determine a new set of

geometrically oriented influence coefficients; subsequently the circulation values were obtained and, finally, a new velocity field. The coordinates of those free vortex segments were then corrected again with slopes generated by new velocities. This process was repeated until further change in coordinates were not in excess of a specified tolerance.

CALCULATION OF FORCES AND MOMENTS

The velocity term in Equation (4) must be determined before the force can be calculated. The procedure is similar to that discussed in the previous section except that the control point has to lie on the vortex segment rather than at the center of a panel, as required by the Kutta-Joukowski theory. Therefore, with reference to Figure 5, the velocity induced at control point 0_ℓ will be the sum of contributions of all vortex segments with known circulation

$$\bar{V}_{0_\ell} = \sum_{K=1}^{N_b} \left[\left(g'_{t_K} \gamma_{t_K} + g'_{ti_K} \gamma_{ti_K} \right) \bar{e}_{vt_K} + \left(g'_{\ell_K} \gamma_{\ell_K} + g'_{\ell i_K} \gamma_{\ell i_K} \right) \bar{e}_{v\ell_K} \right]$$

$$+ \sum_{M=1}^{N_t} \left(g'_{e_M} \gamma_{e_M} + g'_{ei_M} \gamma_{ei_M} \right) \bar{e}_{vt_M} \qquad (29)$$

$$+ \sum_{N=1}^{N_w} \left(g'_{w_N} \gamma_{w_N} + g'_{wi_N} \gamma_{wi_N} \right) \bar{e}_{v\ell_N}$$

where

$$g'_{t_K} = \frac{1}{4\pi h'_{t_K}} \left(\cos \theta'_{t1_K} + \cos \theta'_{t2_K} \right) \qquad (30)$$

$$g'_{ti_K} = \frac{1}{4\pi h'_{ti_K}} (\cos \theta'_{til_K} + \cos \theta'_{ti2_K}) \tag{31}$$

$$g'_{\ell_K} = \frac{1}{4\pi h'_{\ell_K}} (\cos \theta'_{\ell 1_K} + \cos \theta'_{\ell 2_K}) \tag{32}$$

$$g'_{\ell i_K} = \frac{1}{4\pi h'_{\ell i_K}} (\cos \theta'_{\ell il_K} + \cos \theta'_{\ell i2_K}) \tag{33}$$

$$g'_{e_M} = \frac{1}{4\pi h'_{e_M}} (\cos \theta'_{e1_M} + \cos \theta'_{e2_M}) \tag{34}$$

$$g'_{ei_M} = \frac{1}{4\pi h'_{ei_M}} (\cos \theta'_{eil_M} + \cos \theta'_{ei2_M}) \tag{35}$$

$$g'_{w_N} = \frac{1}{4\pi h'_{w_N}} (\cos \theta'_{w1_N} + \cos \theta'_{w2_N}) \tag{36}$$

$$g'_{wi_N} = \frac{1}{4\pi h'_{wi_N}} (\cos \theta'_{wil_N} + \cos \theta'_{wi2_N}) \tag{37}$$

Again, $\theta'_t \ldots$ and $h'_{t_1} \ldots$ are geometrical quantities which can be evaluated as before, but everything is based on control points 0_t and 0_ℓ rather than 0_c.

The force generated at the midpoint of the spanwise segment ac is therefore calculated by using Equation (4)

$$\bar{F}_{0_t} = \rho L_t \Gamma_t \bar{V}_{0_t} \times \bar{e}_{vt} \tag{38}$$

Similarly, the force generated at the midpoint of the chordwise segment ab is

$$\bar{F}_{0_\ell} = \rho L_\ell \Gamma_\ell \bar{V}_{0_\ell} \times \bar{e}_{v\ell} \tag{39}$$

and therefore the resultant total force on a particular panel K is

$$\bar{F}_K = (\bar{F}_{0_t} + \bar{F}_{0_\ell})_K \tag{40}$$

It can also be written in a general form

$$\bar{F}_K = f_{x_K} \bar{i} + f_{y_K} \bar{j} + f_{z_K} \bar{K} \tag{41}$$

The side force and drag coefficients are calculated by summing the force components respectively normal to and parallel to the free stream

$$C_L = \sum_{K=1}^{N_b} (f_{y_K} \cos \alpha - f_{x_K} \sin \alpha) \Big/ \left(\frac{1}{2} \rho V_\infty^2 bc\right) \tag{42}$$

$$C_D = \sum_{K=1}^{N_b} (f_{x_K} \cos \alpha + f_{y_K} \sin \alpha) \Big/ \left(\frac{1}{2} \rho V_\infty^2 bc\right) \tag{43}$$

The moment coefficient with respect to the leading edge is

$$C_{M_{L.E.}} = \sum_{K=1}^{N_b} (f_y x)_K \Big/ \left(\frac{1}{2} \rho V_\infty^2 bc^2\right) \tag{44}$$

and that with respect to the quarter chord is

$$C_{M_{c/4}} = (C_L \cos \alpha + C_D \sin \alpha)\ (C.P. - 0.25) \qquad (45)$$

where C.P. is the center of pressure, i.e.,

$$C.P. = C_{M_{L.E.}} / (C_L \cos \alpha + C_D \sin \alpha) \qquad (46)$$

NUMERICAL RESULTS AND DISCUSSIONS

Numerical results have been obtained for thin rectangular single and double sidewalls with virtual area aspect ratios of 0.05 to 2.0 (or real area aspect ratios of 0.025 to 1.0) at yaw angles up to 12 degrees. For all the cases, the real plane contained 40 panels in the bound vortex lattice, a single tip vortex core and four wake vortex lines. The tip vortex core was divided into 15 segments and each wake vortex line, five segments. The selection of these numbers was a compromise between the accuracy and computer time. The use of other numbers was also investigated and typical results are shown in Figure 6 for the case of AR = 2.0 and α = 12 degrees. The program takes approximately 1 to 1.5 minutes in the CDC 6600 computer for a typical single-wall case and 3 to 4 minutes for a double-wall case. Figure 6 also shows the effect of initial location of the tip vortex core on its shape and the side force coefficient.

SINGLE-SIDEWALL CASES

Figure 7 shows the shape of the tip vortex core and wake vortex lines for a single wall of AR = 2.0 and α = 12 degrees. The final locations of these free vortex lines converged after four iterations. The deflections shown were in the x-y plane only. In the x-z plane which is not shown, the tip vortex core tended to sweep slightly inward until it passed 35 percent of the chord and then outward all the way downstream. The wake vortex lines, on the other hand, swept outward consistently and the outermost line bent the most. The resulting pressure distribution is presented in Figure 8. Note that the leading edge suction was highest close to the center of symmetry. Note also that there was a local positive

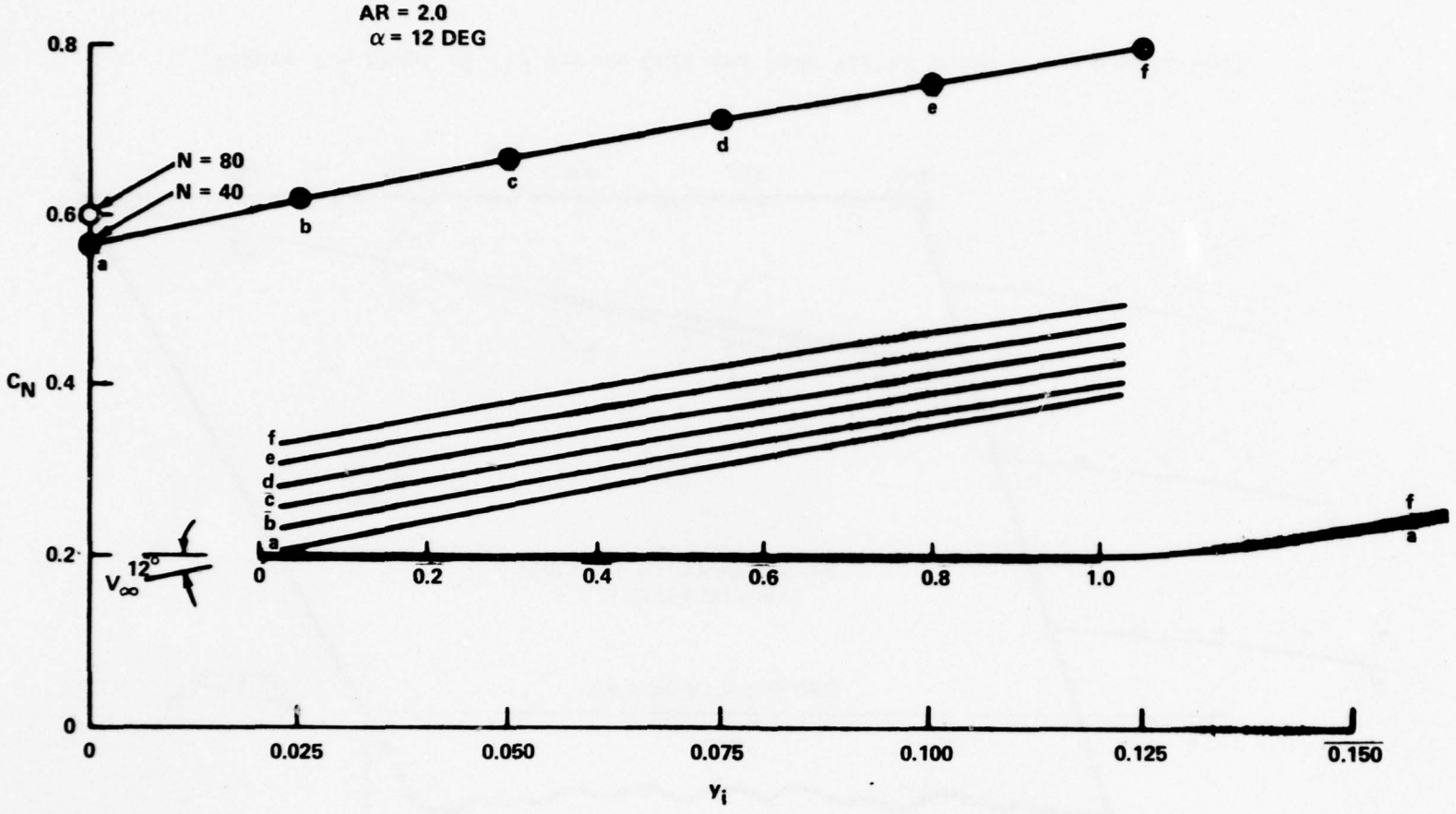

Figure 6 - Effects of Number of Panels of Bound Vortex Sheet and Initial Location of Tip Vortex Core

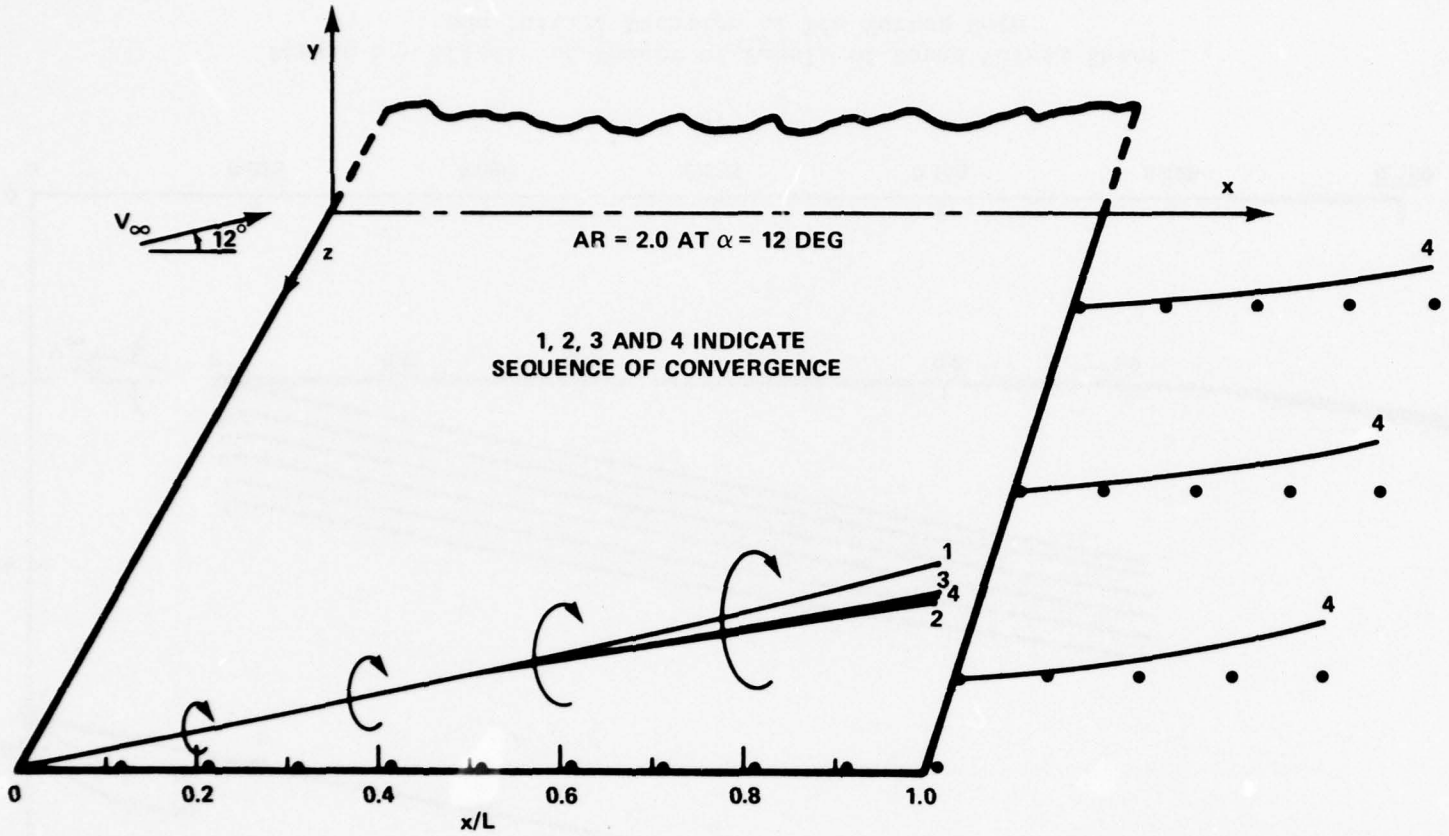

Figure 7 - Shape of Tip Vortex Core and Wake Vortex Lines for a Single Wall

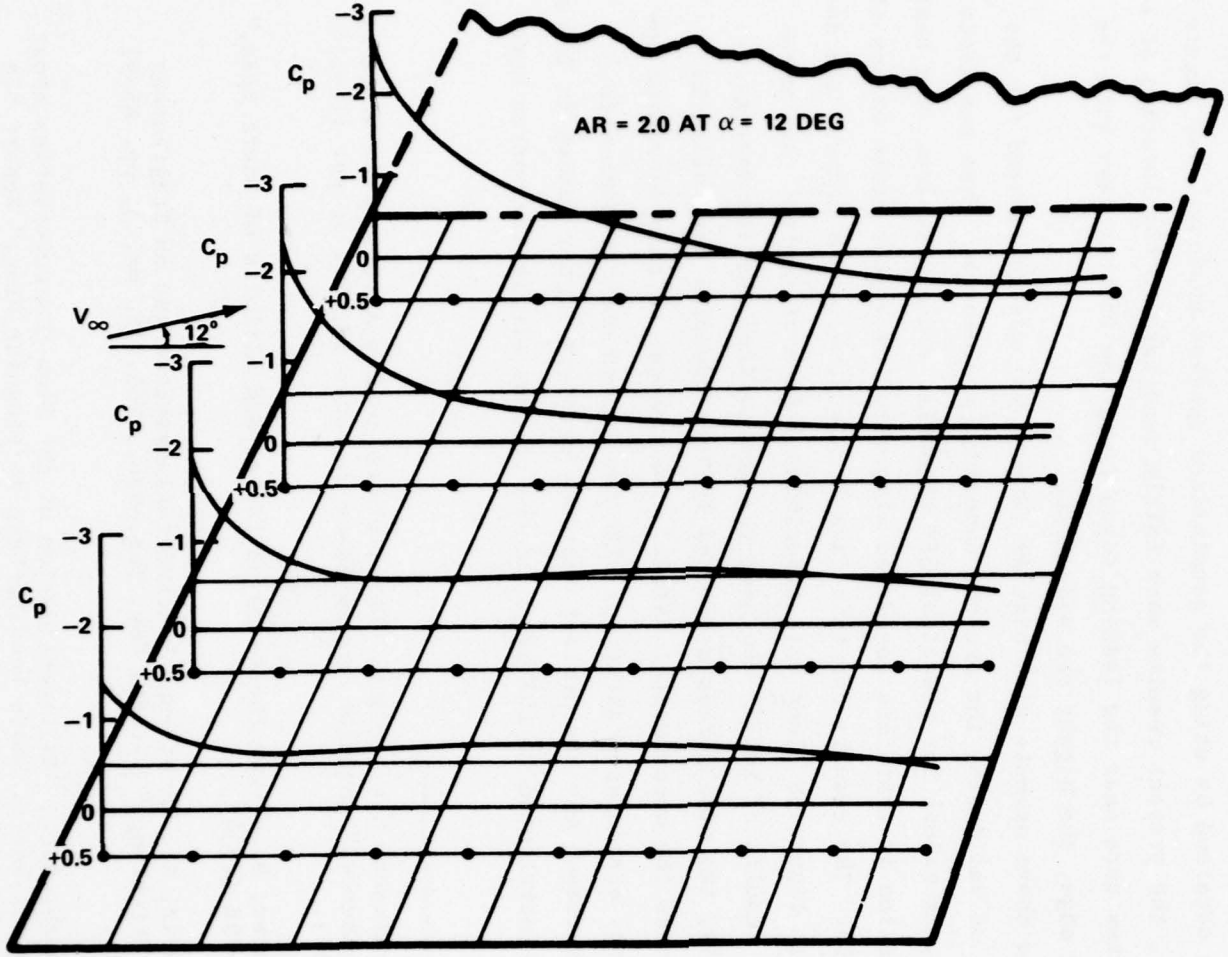

Figure 8 - Pressure Distribution on a Single Wall

pressure region in the downstream area near the center of symmetry. The trend was consistent with that calculated by the three-dimensional potential flow program.[1] The resultant normal force coefficient was in fairly good agreement with experimental data[7-10] and with theoretical results obtained by using the generalized suction analogy;[2] see Figure 9a. However, the present results were fairly sensitive to the location of the tip vortex core near the leading edge; i.e., the farther away from the leading edge, the higher the side force.

The above example with high AR (Figure 9a) was considered for the purpose of validating the present numerical procedures. More realistically, however, AR values for practical SES sidewalls are always low. Our next illustration is therefore concerned with very low aspect ratio values of AR = 0.05. The results for this case at α = 2, 4, and 6 degrees are depicted in Figure 9b along with experimental data of Kaplan[11] and theoretical results of Lamar[2] who used the generalized suction analogy. Generally, the side forces predicted by both theories were slightly higher than the experimental values. The present calculated moment coefficients are in good agreement with the Kaplan experimental data.

The reason why the present approach predicts higher forces in low AR cases is attributed to the limit of the present single tip vortex core

---

[7]Parkinson, G.V. et al., "Observations on Low Aspect Ratio Wings at High Incidence," Canadian Aero & Space J., Vol. 13, No. 3, pp. 111-116 (Mar 1967).

[8]Winter, H., "Flow Phenomena on Plates and Airfoils of Short Span," NACA TM-798 (1936).

[9]Scholz, N., "Kraft-und Druckverteilungsmessungen an Tragflachen kleiner Struckung," Forsch. Geb. Ing.-Wes., Vol. 16, No. 3, pp. 85-91 (1949/50).

[10]Schoch, D.L., "An Investigation of the Flow Characteristics about a Low Aspect Ratio, Sharp Leading-Edge Rectangular Wing," Report 574 (Contract Nonr 1958(14)), D. Aeronautical Eng., Princeton Univ. (Nov 1961); available from DDC as AD 270 111.

[11]Kaplan, P., "An Experimental Study of SES Craft Lateral Hydrodynamic Forces and Moments," Oceanics, Inc. Report 73-97 (May 1973).

Figure 9 - Comparison of Present Single-Sidewall Results with Other Data

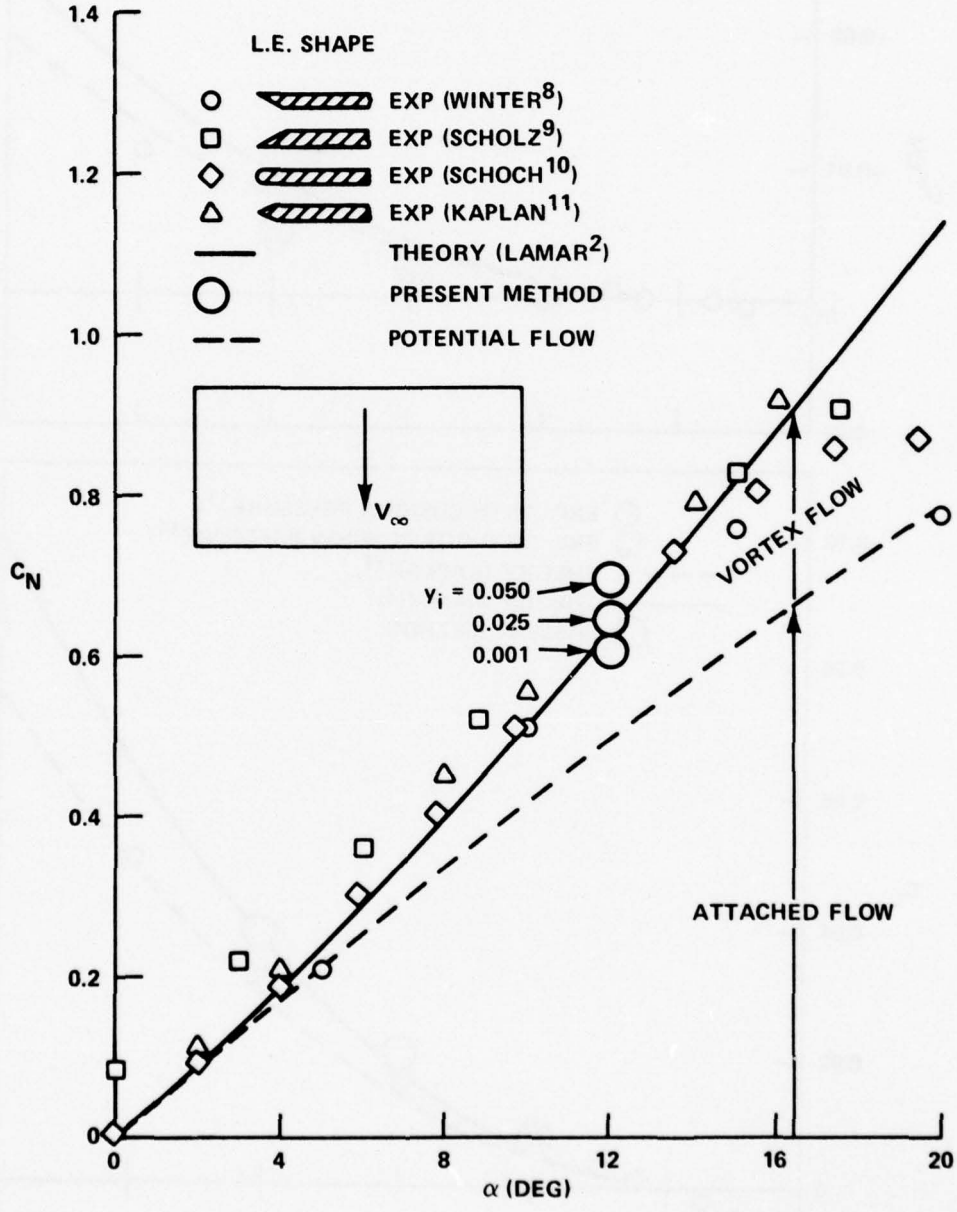

Figure 9a - For AR = 2.0

Figure 9 (Continued)

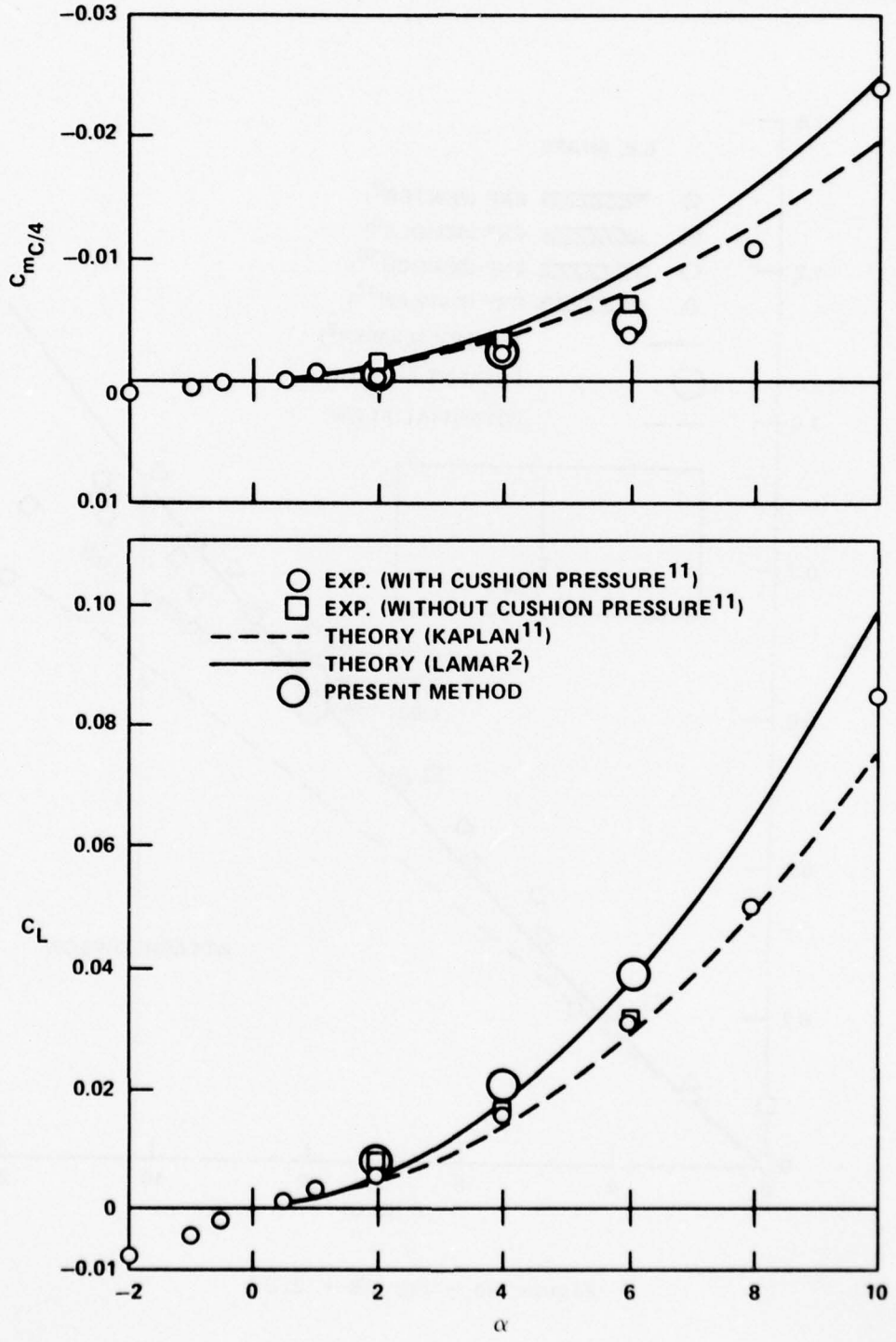

Figure 9b - For AR = 0.05

model. The inaccuracies involved in using a single vortex core to represent a sheet of vorticity rolling up at the sidewall edge are greatest for the induced velocities in the near field, i.e., near the edge of the wall. Since a rectangular wall of low AR value has an "edge region" that is relatively much larger than those of high AR ones, the resultant side force is therefore higher for the former.

DOUBLE-SIDEWALL CASES

Several double-sidewall cases were considered to evaluate the effect of interference due to various arrangements. Area aspect ratios were varied from 0.1 to 0.5 and yaw angles from 2 to 12 degrees. The spacing between two walls was arranged 0.1 to 0.3 chord lengths apart, equivalent to length-over-beam ratios of 3.33 to 10.

Figure 10 indicates the influence of area aspect ratio on side force at α = 6 degrees for different length-over-beam ratios. The interference--as indicated by the difference in C_L values for each sidewall--became more significant as AR increased. This was also true for narrower spacing between the two walls. Figure 10b includes results obtained by Wilson from slender wing theory with the aid of generalized suction analogy.[4] The comparison is rather inconclusive except that both indicate more side force was generated on the upstream sidewall than on the downstream one. The values obtained by Wilson were based on a thickness of 6 percent; no thickness was assumed in the present approach, however.

Figure 11 shows the effect of length-to-beam ratio on the side force at α = 6 degrees for an area aspect ratio AR = 0.1. It is a crossplot of Figures 10a and 10b and so the trend is consistent with those figures. Note that as the L/B value vanished, the side forces on both walls approached the single-wall value. The fact that the present scheme predicts slightly higher side force than given by slender wing theory is attributed to the constraint of the single tip vortex core, as already discussed.

Figure 10 - Effect of Area Aspect Ratio on Side Force

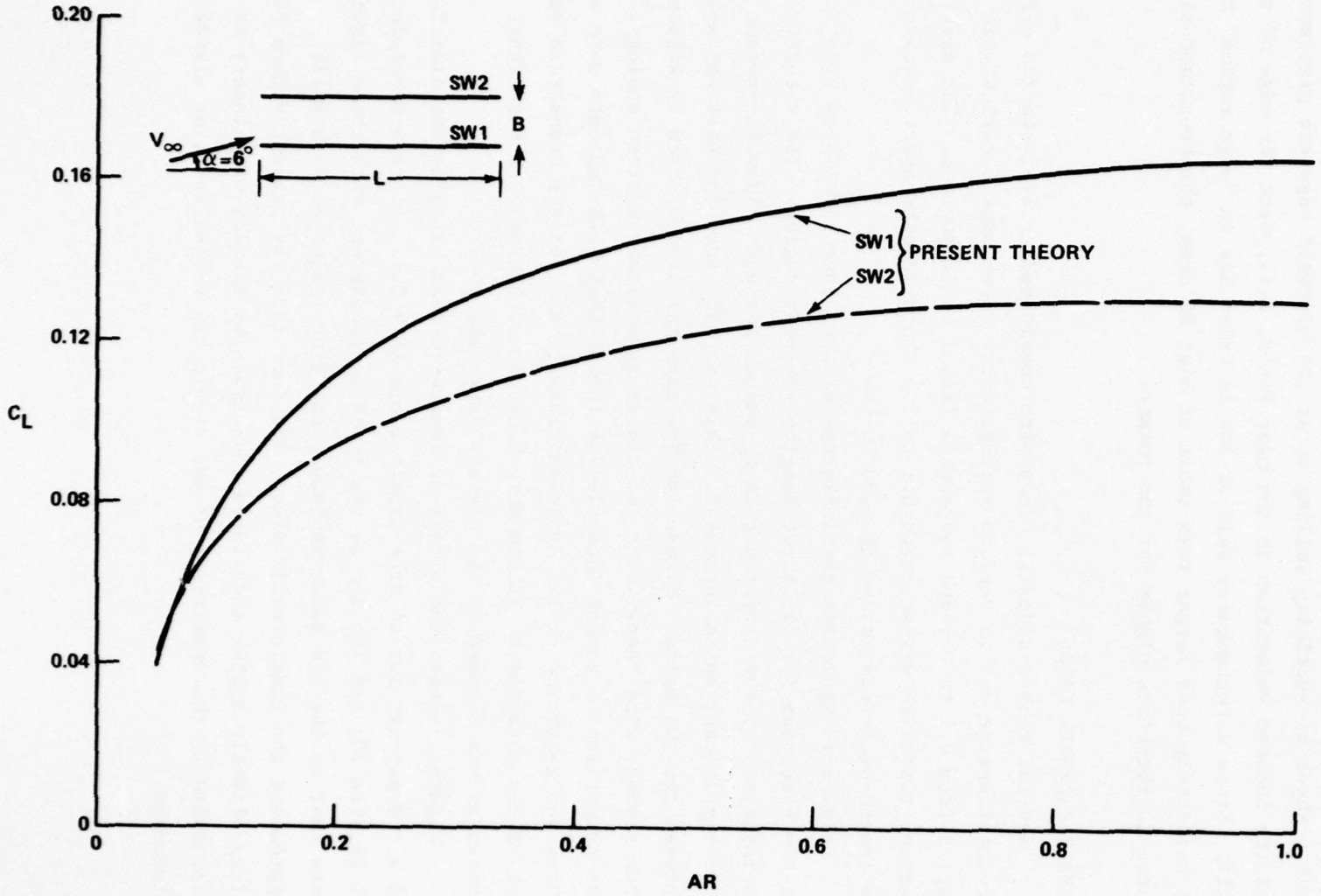

Figure 10a - For L/B = 5 and α = 6 Degrees

Figure 10 (Continued)

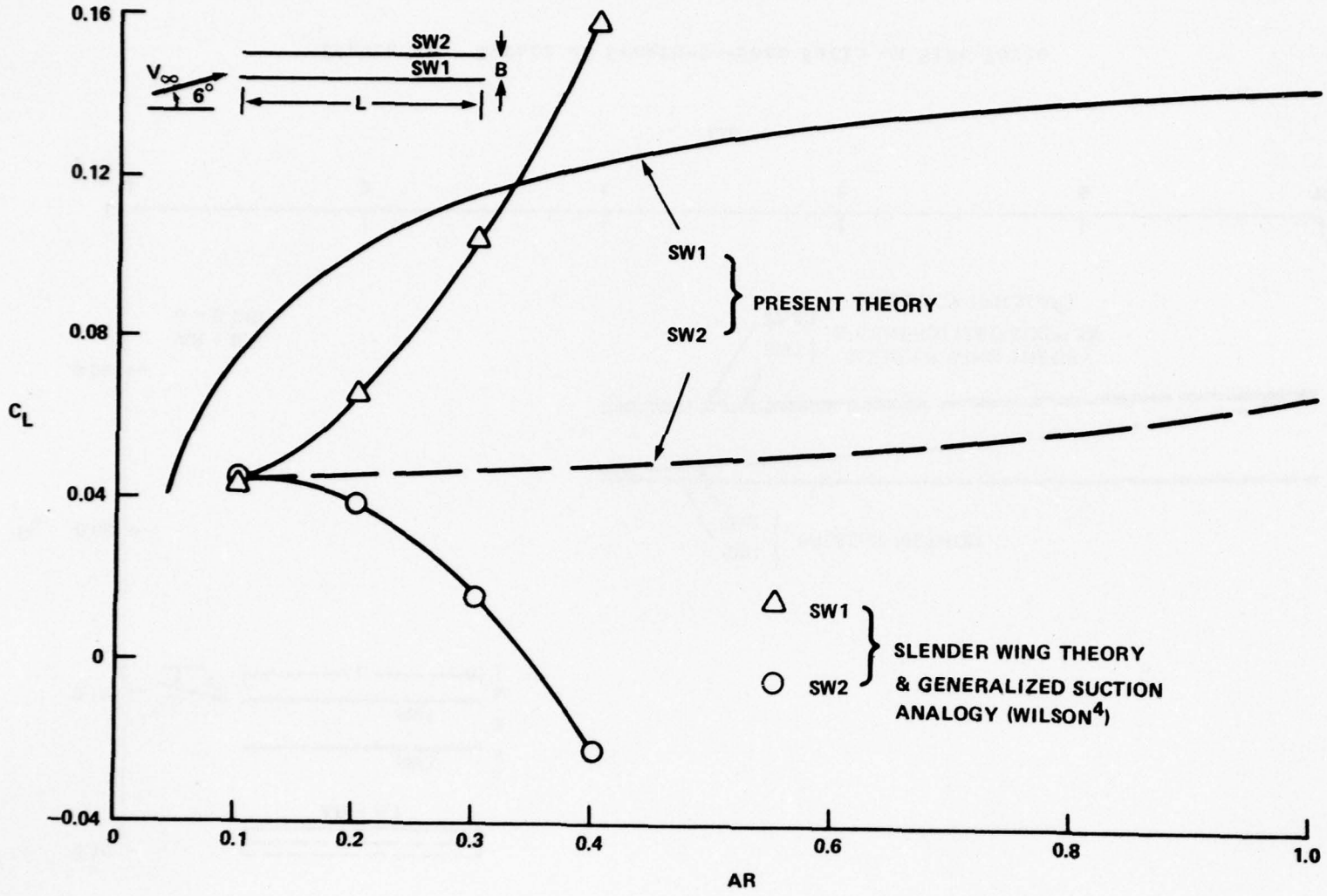

Figure 10b - For L/B = 10 and α = 6 Degrees

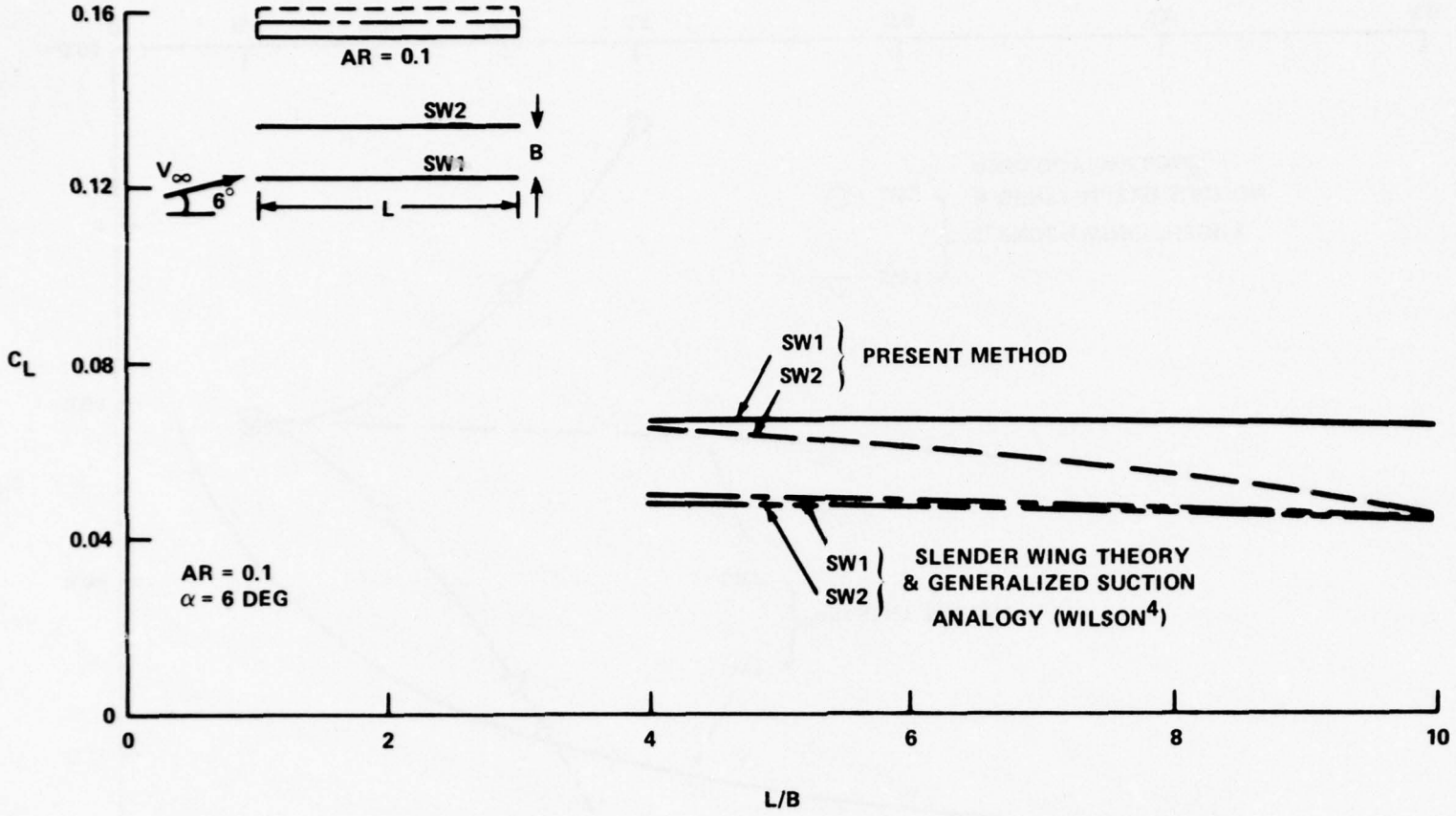

Figure 11 - Effect of Length-to-Beam Ratio on Side Force

Even with interference, the linear relationship between side force and yaw angle held for small aspect ratio cases (AR = 0.1) with moderate length-to-beam ratios (L/B = 5), as observed in Figure 12a. The same was true for the moment. For larger AR values (0.2 to 0.5), however, the linear relationship broke down, as indicated in Figures 12b and 12c and interference became more severe as yaw angle increased. The linearity noted at the lowest aspect ratio is a fortuitous result of the particular aspect ratio, length-to-beam ratio, and the vortex model. It does not indicate any linear asymptotic character of the theory for vanishing aspect ratio.

The above results were generated within the capability of the present single tip vortex core model. The model gave correct information on the force and moment characteristics at various flow conditions and geometric orientations. Because of the unavailability of adequate experimental data for double-sidewall cases, it is impossible to assess the interference effect quantitatively by the present method.

CONCLUSIONS AND RECOMMENDATIONS

A discrete vortex method has been formulated for calculating the forces and moments on SES sidewalls in an inviscid separated flow due to vorticity. Single and double SES sidewalls with different area aspect ratios were considered for various geometrical arrangements and flow conditions. It was found that:

1. The present method predicts higher forces in low aspect ratio cases than do other methods. This is attributed to the use of a single tip vortex model to represent a sheet of vorticity. The dominance of sidewall edge effects reduce accuracy at low aspect ratios. However, accuracy improves with increasing aspect ratio.

2. In the case of double sidewalls, the effect of wall interference becomes significant with increases in length-to-beam ratio, or

Figure 12 - Side Force and Yaw Moment Coefficients at Various Yaw Angles

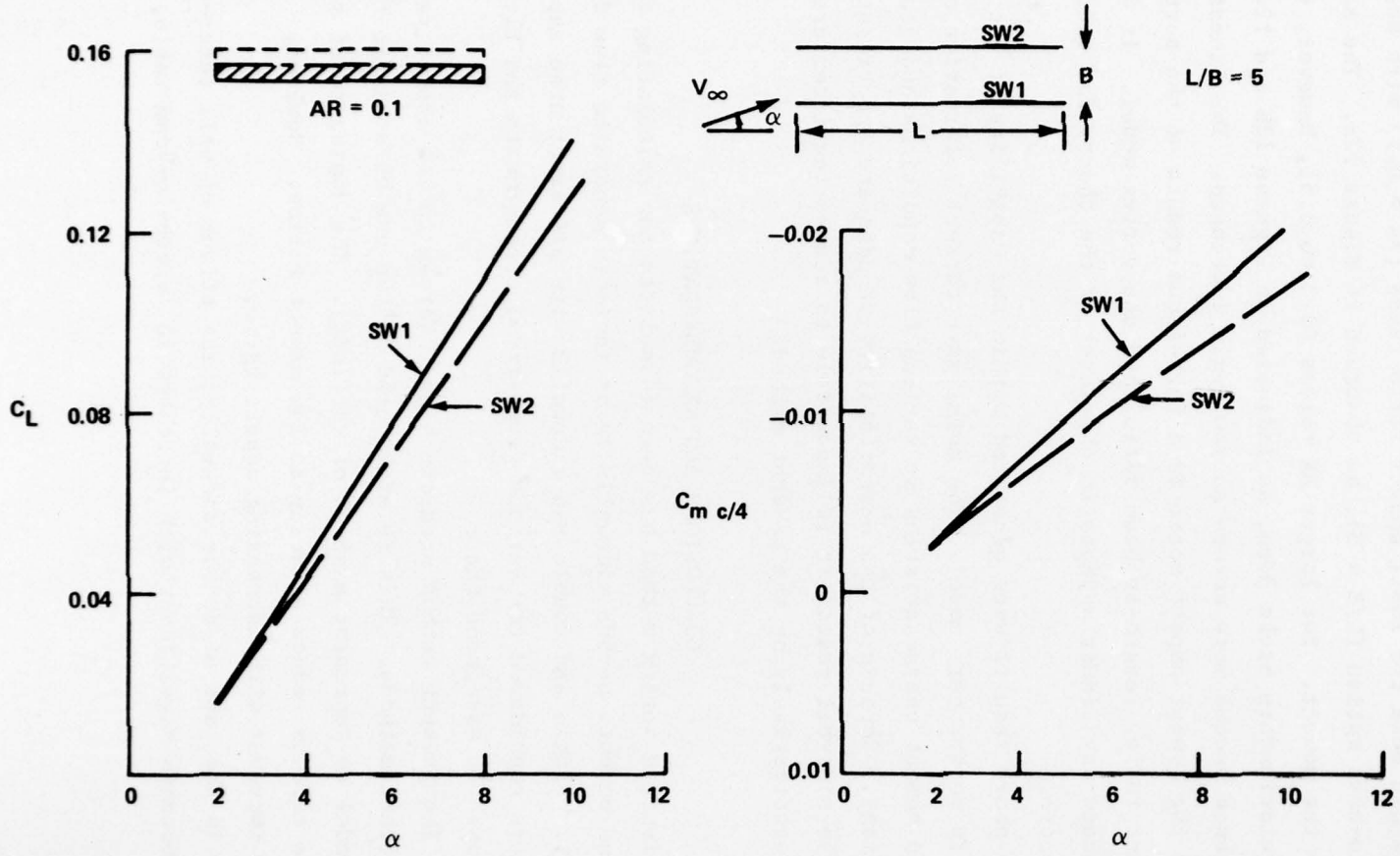

Figure 12a - For AR = 0.1 and L/B = 5

Figure 12 (Continued)

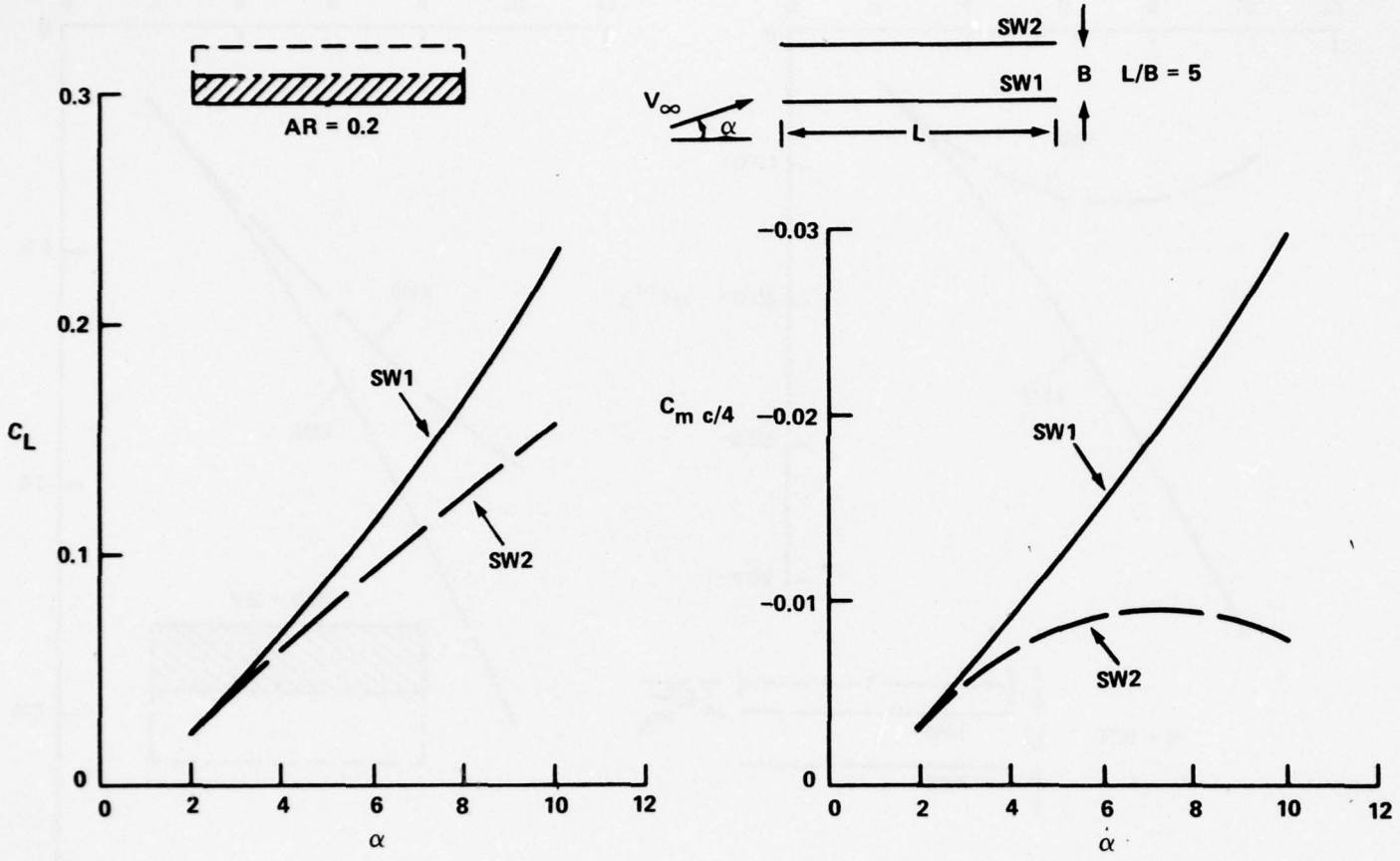

Figure 12b - For AR = 0.2 and L/B = 5

Figure 12 (Continued)

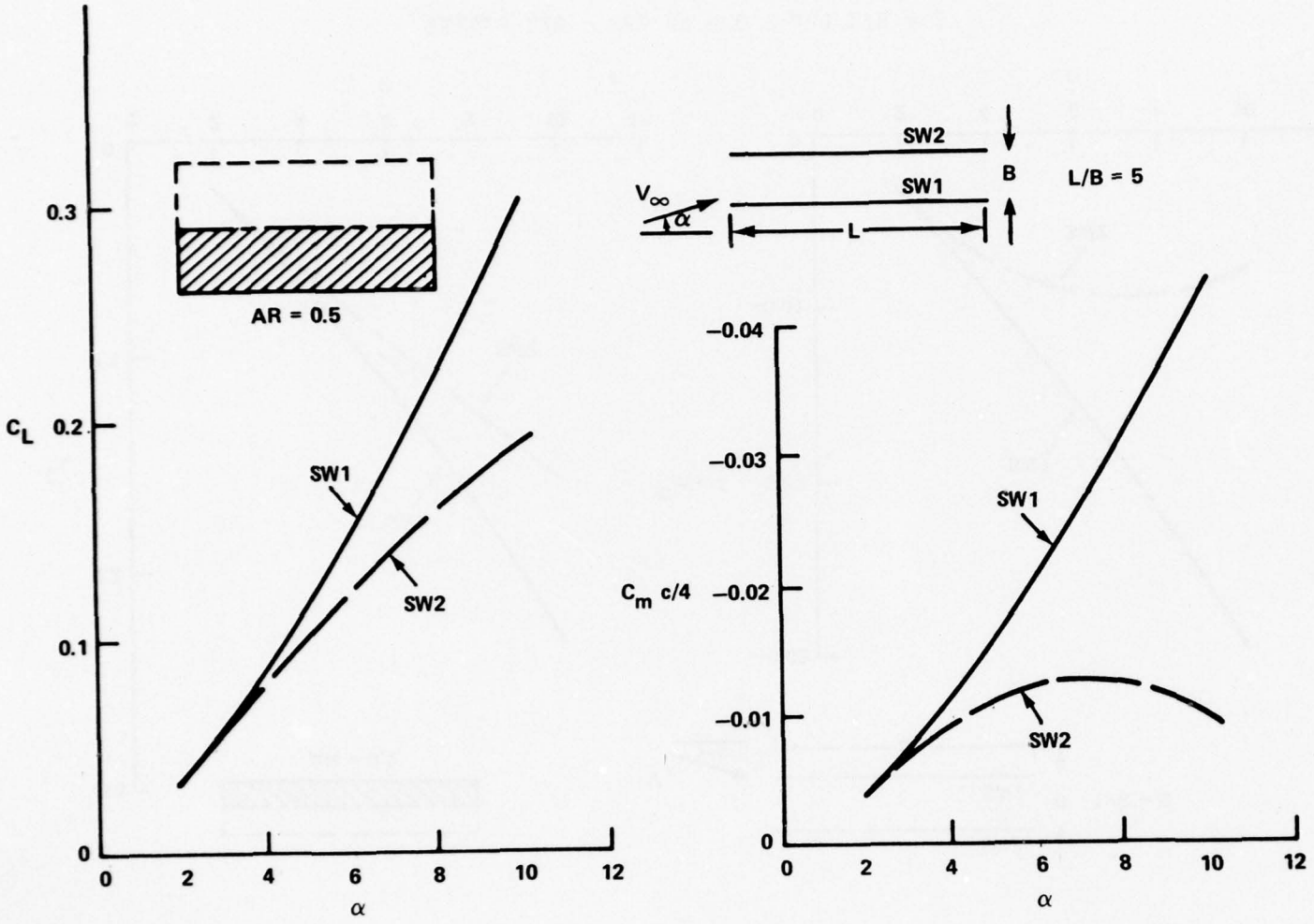

Figure 12c - For AR = 0.5 and L/B = 5

area aspect ratio, or yaw angle. The magnitude of force and moment for either sidewall approaches single-wall values as the length-to-beam ratio diminishes.

In order to extend the method to its full capacity, it is recommended that it be refined to include multitip vortex lines and allow consideration of wall thickness. For verification purposes, experimental investigations should be conducted on double sidewalls in calm water with zero cushion pressure.

APPENDIX

CALCULATION OF INDUCED VELOCITY AND FORCES ASSOCIATED WITH DISCRETE VORTEX METHOD

For a thin SES sidewall traveling at a yaw angle, α, and a pitch angle, β, the flow can be simulated by a bound vortex sheet on the surface of the sidewall and free vortices emanating from the trailing edge and from the edge tip. The schematic of the flow was shown in Figure 1: α is measured with respect to the x-z plane and β with respect to the x-y plane. The $z=0$ plane is assumed to be flat and rigid and its influence is represented by an image in $(-z)$.

A segment in a vortex field serves simultaneously as sender and receiver. A sender induces flow in the surrounding region and a receiver generates velocity as a result of induction from a sender. In a discrete vortex system, a sender or a receiver may consist of more than one straight vortex segment. For convenience, three types of receivers and three types of senders are classified below; they are similar to those developed by Kandil,[5] except the change in z direction.

TYPES OF RECEIVERS

Type 1 Receivers

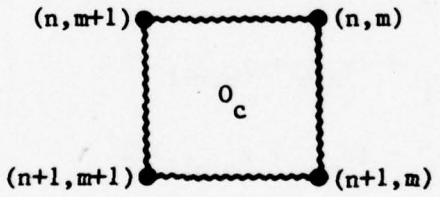

This type of receiver is found in the bound vortex sheet for calculating circulation influence coefficients with center at control point 0_c, whose coordinates are given by

$$x_{0_c} = (x_{n,m} + x_{n,m+1} + x_{n+1,m} + x_{n+1,m+1})/4 \qquad \text{(A-1)}$$

$$y_{0_c} = (y_{n,m} + y_{n,m+1} + y_{n+1,m} + y_{n+1,m+1})/4 \qquad \text{(A-2)}$$

$$z_{0_c} = (z_{n,m} + z_{n,m+1} + z_{n+1,m} + z_{n+1,m+1})/4 \qquad \text{(A-3)}$$

Segment K in Figure 4 is a typical example of a receiver of Type 1. Velocity is computed at control point 0_c.

Type 2 Receivers

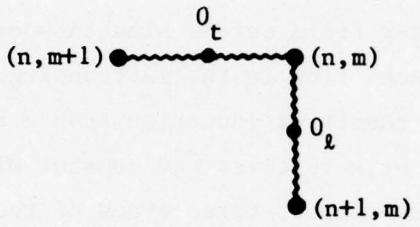

The velocity is calculated at midpoints 0_t and 0_ℓ:

$$x_{0_t} = (x_{n,m} + x_{n,m+1})/2 \qquad \text{(A-4)}$$

$$y_{0_t} = (y_{n,m} + y_{n,m+1})/2 \qquad \text{(A-5)}$$

$$z_{0_t} = (z_{n,m} + z_{n,m+1})/2 \qquad \text{(A-6)}$$

$$x_{0_\ell} = (x_{n,m} + x_{n+1,m})/2 \qquad \text{(A-7)}$$

$$y_{0_\ell} = (y_{n,m} + y_{n+1,m})/2 \qquad \text{(A-8)}$$

$$z_{0_\ell} = (z_{n,m} + z_{n+1,m})/2 \qquad \text{(A-9)}$$

This type of receiver is found in bound vortex for calculating forces as shown in Figure 5.

Type 3 Receivers

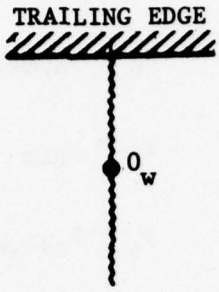

The velocity is calculated at the upstream end of a vortex segment in the wake 0_w:

$$x_{0_w} = x_{n,m}$$

$$y_{0_w} = y_{n,m}$$

$$z_{0_w} = z_{n,m}$$

TYPES OF SENDERS

The vortex elements that induce velocity are called senders. Three different types are illustrated here.

Type 1 Senders

This type of sender is found in the bound vortex lattice for calculating both circulation infuence coefficients and forces.

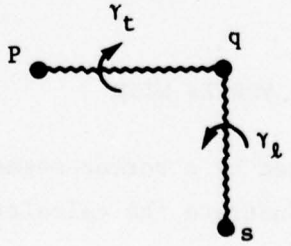

Coordinates of p,q, and s are defined by

$$x_p = x_{n,m+1} \qquad y_p = y_{n,m+1} \qquad z_p = z_{n,m+1}$$

$$x_q = x_{n,m} \qquad y_q = y_{n,m} \qquad z_q = z_{n,m} \qquad \text{(A-10)}$$

$$x_s = x_{n+1,m} \qquad y_s = y_{n+1,m} \qquad z_s = z_{n+1,m}$$

Type 2 Senders

This type is found at the free tip vortex core

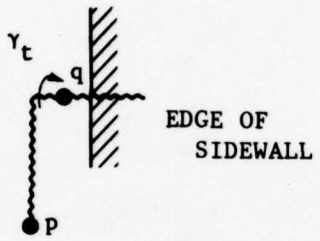

Type 3 Senders

This type is found at the free wake vortex lines

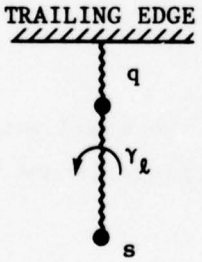

INDUCED VELOCITY ON BOUND VORTEX WITH UNIT CIRCULATION

The velocity generated by a vortex segment is determined by using the Biot-Savart law. To demonstrate the calculation, consider the velocity

on a bound vortex with unit circulation attributed from the bound vortex itself, the tip vortex core, and the wake vortex lines. Within the bound vortex, the computation is concerned with a receiver of Type 1. The step-by-step procedure is as follows:

1. Calculate the induced velocity due to bound vortex

a. The position vectors of the control point (0_c) of the receiver with respect to the ends of the vortex segment of the sender (p,q,s) are:

$$\bar{r}_p = (x_{0_c} - x_p)i + (y_{0_c} - y_p)j + (z_{0_c} - z_p)k$$

$$\bar{r}_q = (x_{0_c} - x_q)i + (y_{0_c} - y_q)j + (z_{0_c} - z_q)k \qquad \text{(A-11)}$$

$$\bar{r}_s = (x_{0_c} - x_s)i + (y_{0_c} - y_s)j + (z_{0_c} - z_s)k$$

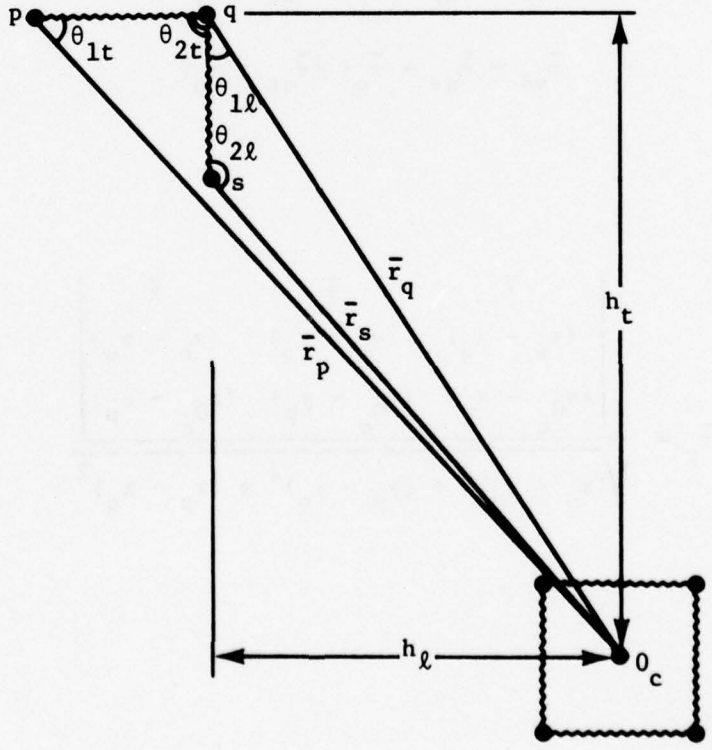

b. The unit vectors parallel to the spanwise and chordwise vortex segments of the sender are:

$$\bar{e}_{qp} = \frac{(x_p - x_q)\bar{i} + (y_p - y_q)\bar{j} + (z_p - z_q)\bar{k}}{\sqrt{(x_p - x_q)^2 + (y_p - y_q)^2 + (z_p - z_q)^2}}$$

$$\bar{e}_{qs} = \frac{(x_s - x_q)\bar{i} + (y_s - y_q)\bar{j} + (z_s - z_q)\bar{k}}{\sqrt{(x_s - x_q)^2 + (y_s - y_q)^2 + (z_s - z_q)^2}} \qquad \text{(A-12)}$$

c. The unit vectors parallel to the velocities generated by the spanwise and chordwise vortex segments are:

$$\bar{e}_{vt} = \bar{e}_{qp} \times \bar{r}_p / |\bar{e}_{qp} \times \bar{r}_p|$$

$$\bar{e}_{v\ell} = \bar{e}_{qs} \times \bar{r}_q / |\bar{e}_{qs} \times \bar{r}_q| \qquad \text{(A-13)}$$

Here

$$\bar{e}_{qp} \times \bar{r}_p = \frac{\begin{vmatrix} \bar{i} & \bar{j} & \bar{k} \\ (x_p - x_q) & (y_p - y_q) & (z_p - z_q) \\ (x_{0_c} - x_p) & (y_{0_c} - y_p) & (z_{0_c} - z_p) \end{vmatrix}}{\sqrt{(x_p - x_q)^2 + (y_p - y_q)^2 \times (z_p - z_q)^2}} \qquad \text{(A.14)}$$

$$\bar{e}_{qs} \times \bar{r}_q = \frac{\begin{vmatrix} \bar{i} & \bar{j} & \bar{k} \\ (x_s - x_q) & (y_s - y_q) & (z_s - z_q) \\ (x_{0_c} - x_q) & (y_{0_c} - y_q) & (z_{0_c} - z_q) \end{vmatrix}}{\sqrt{(x_s - x_q)^2 + (y_s - y_q)^2 + (z_s - z_q)^2}} \qquad \text{(A.15)}$$

and

$$h_t = |\bar{e}_{qp} \times \bar{r}_p| \qquad \text{(A-16)}$$

$$h_\ell = |\bar{e}_{qs} \times \bar{r}_q| \qquad \text{(A-17)}$$

Here Equation (A.16) indicates the distance from the control point to the spanwise segment and Equation (A.17) the distance from the control point to the chordwise segment.

d. The unit normal vector of the receiver is calculated by Equations (24) through (26).

e. The cosines of the angles between the spanwise segment and the position vectors $\bar{r}_p$ and $\bar{r}_q$ are

$$\cos \theta_{1t} = \frac{\bar{e}_{qp} \cdot \bar{r}_p}{|\bar{r}_p|} \qquad \text{(A-18)}$$

$$\cos \theta_{2t} = \frac{-\bar{e}_{qp} \cdot \bar{r}_q}{|\bar{r}_q|} \qquad \text{(A-19)}$$

f. The cosines of the angles between the chordwise segment and the position vectors $\bar{r}_q$ and $\bar{r}_s$ are

$$\cos \theta_{1_\ell} = \frac{\bar{e}_{qs} \cdot \bar{r}_q}{|\bar{r}_q|} \qquad \text{(A-20)}$$

$$\cos \theta_{2\ell} = \frac{-\bar{e}_{qs} \cdot \bar{r}_s}{|\bar{r}_s|} \tag{A-21}$$

g. From the Biot-Savart law, the velocities generated at the control point by the spanwise and chordwise segments (each have unit circulation) are

$$\bar{V}_{t1}(1) = \frac{(\cos \theta_{1t} + \cos \theta_{2t})\, \bar{e}_{vt}}{4\pi h_t}$$

$$\bar{V}_{\ell 1}(1) = \frac{(\cos \theta_{1\ell} + \cos \theta_{2\ell})\, \bar{e}_{v\ell}}{4\pi h_\ell} \tag{A-22}$$

h. The normal component of the velocities at the control point are

$$V_{tn_1}(1) = \bar{V}_{t1}(1) \cdot \bar{e}_n$$

$$V_{\ell n_1}(1) = \bar{V}_{\ell 1}(1) \cdot \bar{e}_n \tag{A-23}$$

i. Velocity generated by the image--since the upper end of the sidewall is attached to the ship, the influence of its flat upper surface is accounted for by the velocity generated by the image of the sender. The coordinates of the image are calculated by simply changing the signs of the z-coordinates of the sender. For instance at control point 0_c, the position vectors with respect to p′, q′, s′ of the sender in the imaginary plane are

$$\bar{r}_{p'} = (x_{0_c} - x_p)\bar{i} + (y_{0_c} - y_p)\bar{j} + (z_{0_c} + z_p)\bar{k}$$

$$\bar{r}_{q'} = (x_{0_c} - x_q)\bar{i} + (y_{0_c} - y_q)\bar{j} + (z_{0_c} + z_q)\bar{k} \qquad \text{(A-24)}$$

$$\bar{r}_{s'} = (x_{0_c} - x_s)\bar{i} + (y_{0_c} - y_s)\bar{j} + (z_{0_c} + z_s)\bar{k}$$

Following a similar procedure, the resulting normal components of the velocities at control point 0_c due to the image are:

$$V_{tn_1}(2) = \bar{V}_{t_1}(2) \cdot \bar{e}_n$$

$$V_{\ell n_1}(2) = \bar{V}_{\ell_1}(2) \cdot \bar{e}_n \qquad \text{(A-25)}$$

j. The total resulting velocity generated at the receiver is the vector sum of those contributed by the senders in the real and image planes. The normal components of the velocities at the control point of the receiver (nr) generated by the sender (ns) and its image are then:

$$V_{tn}(ns,nr) = V_{tn_1}(1) - V_{tn_1}(2)$$

$$V_{\ell n}(ns,nr) = V_{\ell n_1}(1) + V_{\ell n_1}(2) \qquad \text{(A-26)}$$

2. Calculate the induced velocity due to tip vortex

a. The position vectors of control points for receivers of Type 1 with respect to the ends of tip free vortex are:

$$\bar{r}_p = (x_{0_c} - x_p)\bar{i} + (y_{0_c} - y_p)\bar{j} + (z_{0_c} - z_p)\bar{k}$$

$$\bar{r}_q = (x_{0_c} - x_q)\bar{i} + (y_{0_c} - y_q)\bar{j} + (z_{0_c} - z_q)\bar{k} \qquad \text{(A-27)}$$

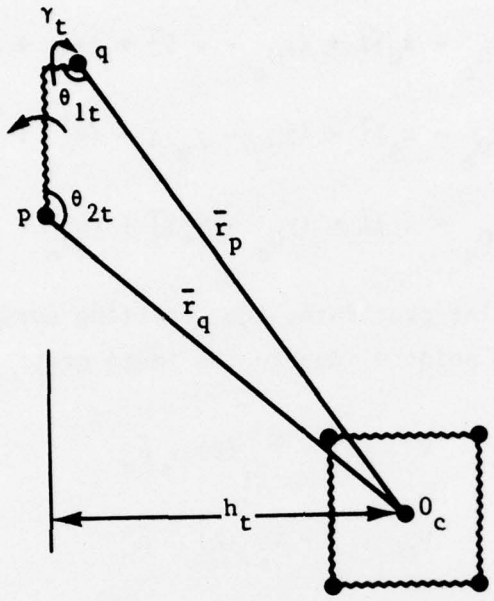

b. The unit vector parallel to the tip vortex segment is:

$$\bar{e}_q = \frac{(x_p - x_q)\bar{i} + (y_p - y_q)\bar{j} + (z_p - z_q)\bar{k}}{\sqrt{(x_p - x_q)^2 + (y_p - y_q)^2 + (z_p - z_q)^2}} \qquad \text{(A-28)}$$

c. The unit vectors parallel to the velocity generated at the control point of Type 1 by the tip vortex segment are:

$$\bar{e}_{vt} = \frac{\bar{e}_{qp} \times \bar{r}_p}{|\bar{e}_{qp} \times \bar{r}_p|} \qquad \text{(A-29)}$$

$$h_t = |\bar{e}_{qp} \times \bar{r}_p| \qquad \text{(A-30)}$$

The second equation indicates the distance from 0_c to the tip vortex segment.

d. The cosines of the angles between the tip vortex segment and the position vectors $\bar{r}_p$ and $\bar{r}_q$ are:

$$\cos \theta_{1t} = \frac{\bar{e}_{qp} \cdot \bar{r}_p}{|\bar{r}_p|} \tag{A-31}$$

$$\cos \theta_{2t} = \frac{-\bar{e}_{qp} \cdot \bar{r}_q}{|\bar{r}_q|} \tag{A-32}$$

e. The velocity generated at the control point by the tip vortex segment with unit circulation is:

$$\bar{V}_{t1}(1) = \frac{(\cos \theta_{1t} + \cos \theta_{2t})\, \bar{e}_{vt}}{4\pi h_t} \tag{A-33}$$

f. The normal component of the velocity at the control point is:

$$V_{tn_1}(1) = \bar{V}_{t1}(1) \cdot \bar{e}_n$$

g. The unit vector parallel to the last tip vortex segment is

$$\bar{e}_{qp} = (\cos \alpha)\bar{i} + (\sin \alpha)\bar{j} \tag{A-34}$$

h. The unit vector parallel to the velocity generated at control point of Type 1 by the last tip vortex segment is

$$\bar{e}_{vt} = \frac{\bar{e}_{qp} \times \bar{r}_q}{|\bar{e}_{qp} \times \bar{r}_q|} \tag{A-35}$$

(Here q is the upstream end point of the last tip vortex.)

$$h_t = |\bar{e}_{qp} \times \bar{r}_q| \tag{A-36}$$

i. The cosines of the angles between the last tip vortex segment and the position vector $\bar{r}_q$ are

$$\cos \theta_{1t} = \frac{(x_{0_c} - x_q) \cos a + (y_{0_c} - y_q) \sin a}{\sqrt{(x_{0_c} - x_q)^2 + (y_{0_c} - y_q)^2 + (z_{0_c} - z_q)^2}} \tag{A-37}$$

$$\cos \theta_{2t} = 1 \tag{A-38}$$

j. The velocity generated at the control point by the last tip vortex segment is

$$\bar{V}_{t_1}(1) = \frac{(\cos \theta_{1t} + 1)\, \bar{e}_{vt}}{4\pi h_t} \tag{A-39}$$

k. The normal component of the velocity at the control point 0_c of a Type 1 receiver is

$$V_{tn_1}(1) = \bar{V}_{t_1}(1) \cdot \bar{e}_n \tag{A-40}$$

l. Velocities generated by the image of the free tip vortex core are obtained by substituting negative z-coordinates for p and q in Equations (A-27) and (A-28). The resulting normal component of the velocity at control point 0_c is

$$V_{tn_1}(2) = \bar{V}_{t_1}(2) \cdot \bar{e}_n \tag{A-41}$$

3. Calculate the induced velocity due to wake vortex segments

a. The position vectors of the control point of Type 1 receiver with respect to a free wake vortex segment are

$$\bar{r}_q = (x_{0_c} - x_q)\bar{i} + (y_{0_c} - y_q)\bar{j} + (z_{0_c} - z_q)\bar{k}$$
$$\bar{r}_s = (x_{0_c} - x_s)\bar{i} + (y_{0_c} - y_s)\bar{j} + (z_{0_c} - z_s)\bar{k} \qquad \text{(A-42)}$$

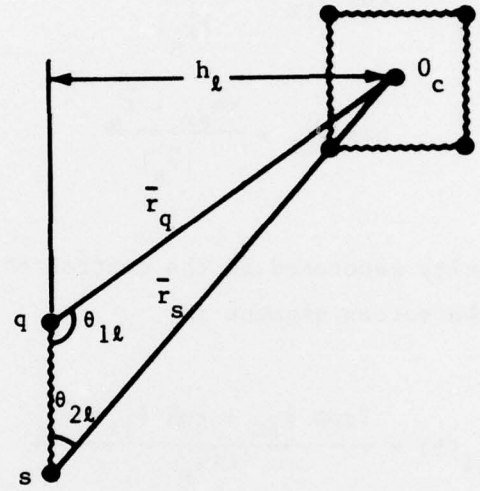

b. The unit vector parallel to the free wake vortex segments is

$$\bar{e}_{qs} = \frac{(x_s - x_q)\bar{i} + (y_s - y_q)\bar{j} - (z_s - z_q)\bar{k}}{\sqrt{(x_s - x_q)^2 + (y_s - y_q)^2 + (z_s - z_q)^2}} \qquad \text{(A-43)}$$

c. The unit vectors parallel to the velocity generated at the control point of a Type 1 receiver by the free wake vortex segment are

$$\bar{e}_{v\ell} = \bar{e}_{qs} \times \bar{r}_q / |\bar{e}_{qs} \times \bar{r}_q| \qquad \text{(A-44)}$$

$$h_\ell = |\bar{e}_{qs} \times \bar{r}_q| \tag{A-45}$$

The second equation indicates the distance from 0_c to the wake vortex segment.

d. The cosines of the angles between the free wake vortex segments and the position vector are

$$\cos \theta_{1\ell} = \frac{\bar{e}_{qs} \cdot \bar{r}_q}{|\bar{r}_q|} \tag{A-46}$$

$$\cos \theta_{2\ell} = \frac{-\bar{e}_{qs} \cdot \bar{r}_s}{|\bar{r}_s|} \tag{A-47}$$

e. The velocity generated at the control point of a Type 1 receiver by the free wake vortex segment is

$$\bar{V}_{\ell 1}(1) = \frac{(\cos \theta_{1\ell} + \cos \theta_{2\ell})\, \bar{e}_{v\ell}}{4\pi h_\ell} \tag{A-48}$$

f. The normal component of the velocity at 0_c is

$$V_{\ell n_1}(1) = \bar{V}_{\ell_1}(1) \cdot \bar{e}_n \tag{A-49}$$

g. The induced velocities due to the last wake vortex segments are

$$\bar{e}_{qs} = (\cos \alpha)\bar{i} + (\sin \alpha)\bar{j} \tag{A-50}$$

$$\bar{e}_{v\ell} = \bar{e}_{qs} \times \bar{r}_s / |\bar{r}_s| \tag{A-51}$$

(here "s" is the upstream end point of the last wake segment.)

$$h_\ell = |\bar{e}_{qs} \times \bar{r}_s| \qquad \text{(A-52)}$$

$$\cos \theta_{1\ell} = \bar{e}_{qs} \cdot \bar{r}_s / |\bar{r}_s|$$

$$\cos \theta_{2\ell} = 1 \qquad \text{(A-53)}$$

$$\bar{V}_{\ell_1}(1) = \frac{(\cos \theta_{1\ell} + \cos \theta_{2\ell})\, \bar{e}_{v\ell}}{4\pi h_\ell} \qquad \text{(A-54)}$$

$$V_{\ell n_1}(2) = \bar{V}_{\ell_1}(2) \cdot \bar{e}_n \qquad \text{(A-55)}$$

h. The induced velocities due to the image of the wake vortex are obtained by substituting negative z-coordinates for q and s in Equations (A-42) to (A-43). The resulting normal component of the velocity at control point 0_c is

$$V_{\ell n_1}(2) = \bar{V}_{\ell_1}(2) \cdot \bar{e}_n \qquad \text{(A-56)}$$

CALCULATION OF FORCES IN BOUND VORTEX

Because of length involvement, the velocity term in the force equation has to be calculated at the middle point of each vortex segment rather than at the geometric center of each panel, as in the previous section. With reference to the following sketch, therefore, the position vector of control point 0_t of a Type 2 receiver with respect to end point p, of the sender is, for instance:

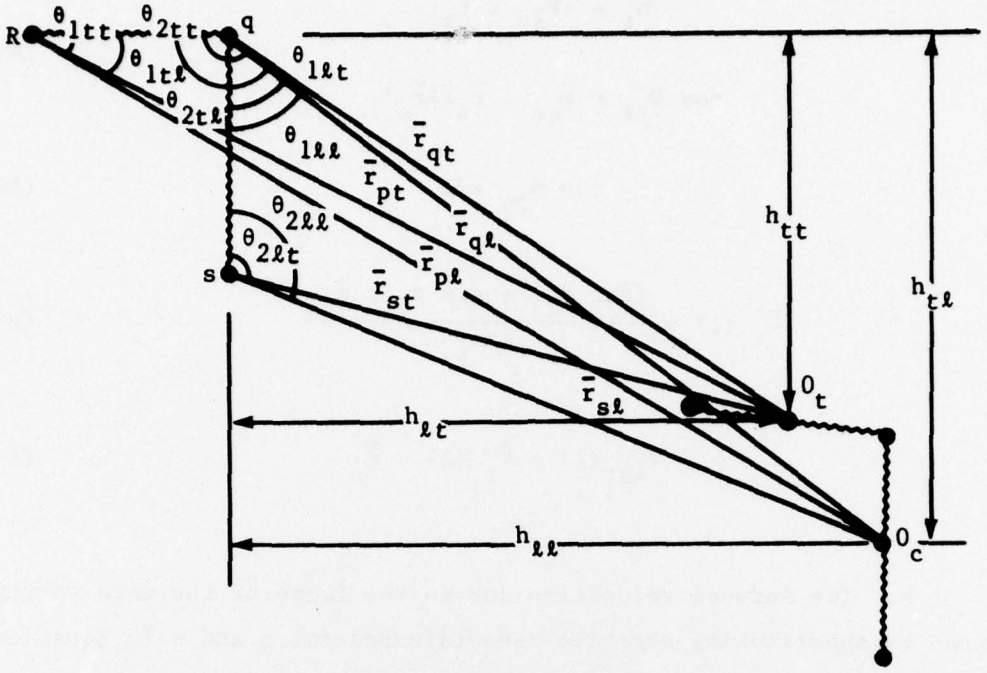

$$\bar{r}_{pt} = (x_{0_t} - x_p)i + (y_{0_t} - y_p)j + (z_{0_t} - z_p)k \qquad \text{(A-57)}$$

Other position vectors $\bar{r}_{p\ell}$, $\bar{r}_{qt}$, $\bar{r}_{q\ell}$, $\bar{r}_{st}$, and $\bar{r}_{s\ell}$ assume similar forms.

The unit vectors parallel to the spanwise and chordwise vortex segments of the sender, $\bar{e}_{qp}$ and $\bar{e}_{qs}$, and unit vectors parallel to the velocity generated at midpoints of Type 2 senders by spanwise and chordwise vortex segments $\bar{e}_{vtt}$, $\bar{e}_{v\ell t}$, $\bar{e}_{vt\ell}$, and $\bar{e}_{v\ell\ell}$ are then obtained by substituting Equations (A-57) through (A-62) for the form of Equation (A-13). Likewise, the velocity at a spanwise receiver of Type 2 due to a spanwise sender is

$$\bar{V}_{tt}(1) = \frac{\gamma_t(ns)\ (\cos\theta_{1tt} + \cos\theta_{2tt})}{4\pi h_{tt}}\ \bar{e}_{vtt} \qquad \text{(A-58)}$$

and the velocity at a spanwise receiver of Type 2 due to a chordwise sender is

$$\bar{V}_{\ell t}(1) = \frac{\gamma_{\ell}(ns)\ (\cos\theta_{1\ell t} + \cos\theta_{2\ell t})}{4\pi h_{\ell t}}\ \bar{e}_{v\ell t} \qquad \text{(A-59)}$$

and the velocity at a chordwise receiver of Type 2 due to a spanwise sender is

$$\bar{V}_{t\ell}(1) = \frac{\gamma_{t}(ns)\ (\cos\theta_{1t\ell} + \cos\theta_{2t\ell})}{4\pi h_{t\ell}}\ \bar{e}_{v\ell t} \qquad \text{(A-60)}$$

and the velocity at a chordwise receiver of Type 2 due to a chordwise sender is

$$\bar{V}_{\ell\ell}(1) = \frac{\gamma_{\ell}(ns)\ (\cos\theta_{1\ell\ell} + \cos\theta_{2\ell\ell})}{4\pi h_{\ell\ell}}\ \bar{e}_{v\ell t} \qquad \text{(A-61)}$$

where the cosines are determined in a manner similar to Equations (A-18) and (A-19) with new position vectors.

Image contributions are obtained by changing the sign of z-coordinates and are designated by "2."

Finally, the velocities at the midpoints 0_t and 0_{ℓ} of the receiver of Type 2 by the sender of Type 1 and its image are

$$V_{0_t} = v_{tt}(1) - v_{tt}(2) + v_{\ell t}(1) - v_{\ell t}(2) \qquad \text{(A-62)}$$

$$V_{0_{\ell}} = v_{t\ell}(1) - v_{t\ell}(2) + v_{\ell\ell}(1) - v_{\ell\ell}(2) \qquad \text{(A-63)}$$

The forces generated at midpoints 0_t and 0_ℓ are then calculated by using the Kutta-Joukowski theory

$$\bar{F}_{0_t} = \rho L_t(nr)\ \gamma_t(nr)\ [\bar{v}_{0_t} \times \bar{e}_t] \tag{A-64}$$

$$\bar{F}_{0_\ell} = \rho L_\ell(nr)\ \gamma_\ell(nr)\ [\bar{v}_{0_\ell} \times \bar{e}_\ell] \tag{A-65}$$

where $L_t(nr)$ and $L_\ell(nr)$ are the lengths of spanwise and chordwise segments of the receiver, respectively.

The forces in bound vortex due to tip and wake vortices are then calculated by following a similar procedure.

EXTENSION OF THE METHOD TO DOUBLE-SIDEWALL CASES

The method has been extended to double-sidewall cases in accordance with the step-by-step procedure outlined below. Since the velocity and force equations are very similar in nature to those presented previously, they will not be repeated here.

1. Bound vortex lattices for both sidewalls lie in x-z planes. The second sidewall is placed above the first one at y = B.

2. The velocities with unknown circulation in bound vortex on Wall 1 due to bound, tip and wake vortices of Walls 1 and 2 are calculated.

3. The velocities with unknown circulation in bound vortex on Wall 2 due to bound, tip and wake vortices of Walls 1 and 2 are calculated.

4. The circulation values γ are determined by solving the influence coefficients.

5. The shape of the tip and wake vortex lines of Wall 1 are then updated.

6. The shape of tip and wake vortex lines of Wall 2 are then updated.

7. Finally, the forces in bound vortices on Walls 1 and 2 are calculated.

REFERENCES

1. Whitehead, R.E., "A Theoretical Prediction Technique for Lateral Hydrodynamic Loads on Sidewalls of Surface Effect Ships," DTNSRDC Report 4766 (Dec 1975).

2. Lamar, J.E., "Extension of Leading-Edge Suction Analogy to Wings with Separated Flow Around the Side Edges at Subsonic Speeds," NASA TR R428 (Oct 1974).

3. Woodward, R.A. et al., "A Computer Program for Three-Dimensional Lifting Bodies in Subsonic Inviscid Flow," United States Army Air Mobility R&D Laboratory Report TR-74-18 (Apr 1974).

4. Wilson, M.B., "Interference Effects on Lateral Forces and Moments on High L/B SES Arrangements," Paper 76-859 presented at the AIAA/SNAME Advanced Marine Vehicles Conference, Arlington, Virginia (Sep 1976).

5. Kandil, O.A., "Prediction of the Steady Aerodynamic Loads on Lifting Surfaces Having Sharp-Edge Separation," Ph.D. Thesis, Virginia Polytechnic Institute and State University, Blacksburg, Va. (Dec 1974).

6. Prandtl, L. and O.E. Tietjens, "Fundamentals of Hydro- and Aerodynamics," translated by L. Rosenhead, Dover Publications, New York (1957).

7. Parkinson, G.V. et al., "Observations on Low Aspect Ratio Wings at High Incidence," Canadian Aero & Space J., Vol. 13, No. 3, pp. 111-116 (Mar 1967).

8. Winter, H., "Flow Phenomena on Plates and Airfoils of Short Span," NACA TM-798 (1936).

9. Scholz, N., "Kraft-und Druckverteilungsmessungen an Tragflachen kleiner Streckung," Forsch. Geb. Ing.-Wes., Vol. 16, No. 3, pp. 85-91 (1949/50).

10. Schoch, D.L., "An Investigation of the Flow Characteristics About a Low Aspect Ratio, Sharp Leading-Edge Rectangular Wing," Report 574 (Contract Nonr 1958(14), D. Aeronautical Eng., Princeton Univ., (Nov 1961); available from DDC as AD 270 111.

11. Kaplan, P., "An Experimental Study of SES Craft Lateral Hydrodynamic Forces and Moments," Oceanics, Inc., Report 73-97 (May 1973).

INITIAL DISTRIBUTION

Copies	
1	ARMY CHIEF OF RES & DEV
1	ARPA
3	CHONR 1 ONR 211 1 ONR 430B 1 ONR 438
3	ONR 1 Boston 1 Chicago 1 Pasadena
1	USNA LIB
1	NAVPGSCOL LIB
1	NAVWARCOL
1	NAVAIRSYSCOM
3	NAVSEA 1 03512
1	NASEC, 6110
1	NADC
1	PM 17
1	NSWC WHITE OAK
1	NSWC DAHLGREN LAB/LIB
12	DDC
1	AFFDL
1	AFOSR
1	AFIT
1	AEDC
4	NASA 1 HQS NASA 1 NASA AMES RES CEN

Copies	
	1 NASA LANGLEY RES CEN 1 NASA LEWIS RES CEN
1	NSF
1	POLY INST OF BROOKLYN/GRAD CEN LIB
1	BROWN U/DIV ENGR
1	U CAL BERKELEY/PROF M. HOLT
1	UC SAN DIEGO/DEPT AERO ENGR
2	CIT 1 AERO LIB 1 PROF T. KUBOTA
1	CATHOLIC U/TECH LIB
1	CLEMSON U
1	CORNELL U
1	GEORGIA INST OF TECHNOL
1	HARVARD U, MCKAY LIB
1	JOHNS HOPKINS U
1	U ILLINOIS, COLL ENGR
2	U MARYLAND 1 LIB 1 DR. S.I. PAI
1	MIT, PARSONS LAB
1	U of MICHIGAN, DEPT ENGR MECH
1	NEW YORK U
1	UNC
1	OHIO STATE U
1	PENN STATE U/DEPT AERO ENGR

Copies	
1	PRINCETON U/DEPT AERO SCI
1	PURDUE U/DEPT AERO ENGR
1	STANFORD U
1	U TENNESSEE, SPACE INST
1	U of VA
1	VIRGINIA POLY INST & ST U 1 NEWMAN LIB
1	WEST VIRGINIA U
1	AIAA
1	DOUGLAS AIRCRAFT

CENTER DISTRIBUTION

Copies	Code	
30	5214.1	Reports Distribution
1	522.1	Library (C)
1	522.2	Library (A)
2	522.3	Aero Lib